Int J Earth Sci (Geol Rundsch) (2006) 95: 871–901
DOI 10.1007/s00531-006-0072-z

ORIGINAL PAPER

Surendra P. Verma

Extension-related origin of magmas from a garnet-bearing source in the Los Tuxtlas volcanic field, Mexico

Received: 16 May 2005 / Accepted: 12 December 2005 / Published online: 5 April 2006

Abstract The Los Tuxtlas volcanic field (LTVF) of late Miocene to Recent age is a key area to understand the consequences of the current subduction of the Cocos plate beneath the North American plate, as well as the competing effects of the ongoing extension along the Gulf of Mexico coast. Geochemical and radiogenic (Sr, Nd, and Pb) isotope data are used to constrain the origin of these 7 Ma to Recent magmas in this area. The basanitic and alkaline basaltic rocks show highly steep light rare-earth element-enriched patterns implying residual garnet in their mantle source, whereas the evolved alkaline and sub-alkaline rocks have less steep rare-earth element patterns consistent with a contribution from the continental crust. Geochemical and isotope data from the LTVF are compared with those from continental rifts, extension-related areas, continental break-up regions, and island and continental arcs, including the Central American volcanic arc related to the subduction of the same oceanic plate (Cocos plate), as well as with those from the two nearby Mexican provinces [the Eastern Alkaline Province (EAP) and the eastern part of the Mexican Volcanic Belt (E-MVB)]. These data for the LTVF primitive rocks are similar to rifts, extension-related areas and continental break-up regions, including the two Mexican provinces, but different from island and continental arcs, including the northern part of the Central American Volcanic Arc (CAVA). The LTVF rocks show an unusual Th and U enrichment with respect to Ba and Rb, which also renders a distinct negative Nb anomaly (with respect to Th and K) in them. These rocks also show a negative Nb anomaly (with respect to Ba and La) that is similar to numerous rift, extension-related areas, and continental break-up regions, but distinct from all arcs around the world, indicating that the magma genesis processes in the LTVF are similar to those in rifts. The "Sr-shift", shown to be a typical feature of most, if not all, island and continental arcs including the CAVA, is not present in the LTVF rocks. Numerous discrimination diagrams, including the new discriminant function diagrams, suggest a rift setting for the LTVF. An essentially extension-related origin of the LTVF is, therefore, inferred in this study. Furthermore, in the light of major and trace element data for LTVF primitive rocks and their modelling an incompatible element-enriched garnet-bearing source seems plausible. The LTVF source is likely to reside in the lithosphere rather than the asthenosphere although the asthenospheric contribution cannot be completely ruled out. The evolved alkaline and sub-alkaline rocks might have a lower crustal component. Finally, it appears that the LTVF shows more affinity to the EAP rather than to the Mexican Volcanic Belt (MVB), implying that the LTVF should probably be considered as a part of the EAP.

Keywords Geochemistry · Rift · Subduction · Mexico · Central American Volcanic Arc · Eastern Alkaline Province · Mexican Volcanic Belt · Island arc · Continental arc

S. P. Verma
Centro de Investigación en Energía, UNAM,
Priv. Xochicalco s/no., Col. Centro, Apartado Postal 34,
Temixco, Morelos, 62580, Mexico
E-mail: spv@cie.unam.mx
Tel.: +52-55-56229745
Fax: +52-777-3250018

Introduction

The Los Tuxtlas volcanic field (LTVF) is an isolated area of volcanic centres (cinder cones and stratovolcanoes) of Late Miocene (~7 Ma) to Recent age located on the Gulf of Mexico coastal plain (Fig. 1; see Nelson et al. 1995 for more details on the LTVF). It lies about 200 km SE of the easternmost part of the E–W oriented Mexican Volcanic Belt (MVB) and about 400 km NE of the NW–SE oriented Central American Volcanic Arc (CAVA). Between the LTVF and MVB, volcanism is absent, whereas between the LTVF and CAVA, only some isolated volcanic centres, such as the El Chichón volcano, are present. In relation to the subducting or

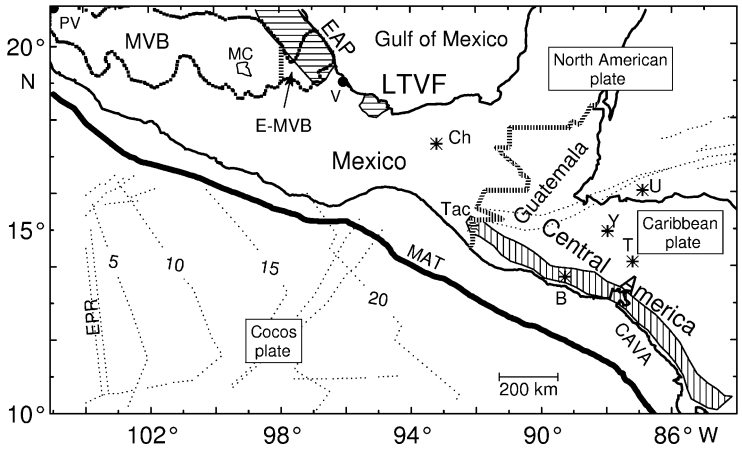

Fig. 1 Location of Miocene to Recent volcanism in the Los Tuxtlas volcanic field (*LTVF*), the Mexican Volcanic Belt (*MVB*), part of the Eastern Alkaline Province (*EAP*) and the Central American Volcanic Arc (*CAVA*). The eastern part of the MVB (*E-MVB*) is schematically shown by a *vertical, heavy, line*; note also the overlap region of the easternmost MVB with the EAP. The plate tectonic relationship of the subducting or downgoing Cocos plate with the North American and Caribbean plates is also shown. The curves marked *5*, *10*, *15* and *20* show the approximate age of the ocean crust in Ma. *MAT* Middle America Trench, *EPR* East Pacific Rise. The volcanoes shown are: *Ch* El Chichón volcano, *Tac* Tacaná volcano, *B* Boqueron volcano, *T* Tegucigalpa volcano, *Y* Yohoa volcano, *U* Utila Island. The cities are: *MC* Mexico City, *V* Veracruz, *PV* Puerto Vallarta

downgoing Cocos plate, the "volcanic front" of the LTVF lies ~320 km from the Middle America trench (MAT), whereas the LTVF volcanoes near the Gulf of Mexico coast are located ~400 km from this trench (Fig. 1).

The MVB is a geologic province of ~8,000 volcanic centres (stratovolcanoes, cinder cones, maars, etc.) of Miocene to Recent age, ~1,000 km long and ~50–300 km wide, extending approximately east–west from Veracruz to Puerto Vallarta and making an angle of ~20° with respect to the MAT (Fig. 1). Its origin is presumably related to the subduction of the Cocos plate beneath the North American plate (e.g. Robin 1982a; Pardo and Suárez 1995) although this "subduction relationship" of the MVB has now been questioned (for more details see Verma 2002, 2004 and references cited therein).

The CAVA is a late Tertiary–Quaternary volcanic province, sub-parallel to the MAT, ~1,100 km long, extending from Mexico–Guatemala border to central Costa Rica, and is related to the subduction of the Cocos plate beneath the Caribbean plate (Carr et al. 1982). Although Central American continental margin shows a well-defined, wide fore-arc basin (see the wide area between the MAT and CAVA in Fig. 1), the Mexican continental margin is characterized by a steep continental slope and a narrow shelf (von Huene 1989). These morphological differences between the Mexican and Central American parts of the trench might have consequences for volcanism on-land (Verma 2004).

The north–south trending Eastern Alkaline Province (EAP) with abundant alkaline rocks is related to extensional faults adjacent to the Gulf of Mexico (Fig. 1; Robin 1976, 1982b). On the basis of limited age data, Robin and colleagues (Robin and Tournon 1978; Cantagrel and Robin 1979; Robin 1982b) also suggested that magmatism in the EAP has extended from the Rio Grande Rift (USA), southward from near the USA–Mexico border during the Miocene to as far south as the LTVF during the Plio-Quaternary, implying that the LTVF belongs to the EAP.

The LTVF is considered to be a key area to understand the competing effects of subduction of the Cocos plate beneath the North American plate and those of ongoing extension along the Gulf of Mexico coast. Depth contours of the subducted Cocos plate (e.g. Burbach et al. 1984; Singh and Pardo 1993; Pardo and Suárez 1995) show that this plate subducts "sub-horizontally" beneath the North American plate, but does so at a much steeper angle beneath the Caribbean plate. According to Lomnitz (1982) the downgoing slab is seismically defined to only about 80–100 km depth, and it becomes sub-horizontal beneath the LTVF area. Pardo and Suárez (1995), on the other hand, using mainly local seismic data (without stating their reliability) claimed to have defined the downgoing slab in this area to depths of about 120 km. In any case, with the LTVF lying very far (about 320–400 km) from the trench, the downgoing slab can still be considered as "sub-horizontal" (subduction angle of only ~15°).

The origin of the LTVF is of great interest because it is situated in this anomalous setting and because its origin has been controversial: the existing models vary from a simple subduction relationship (according to Thorpe 1977), to a more complex situation in which both arc and back-arc are located in the same LTVF area (according to Nelson et al. 1995), and to the extensional tectonics along the Gulf of Mexico coastal region (according to Robin and co-workers) as discussed below.

From petrographic description and chemical analyses of lavas from the LTVF, Friedländer and Sonder (1923) were the first to point out that these lavas were dominantly basaltic, including some picrites and andesites. Pichler and Weyl (1976) concluded that the LTVF rocks are dominantly alkaline, although tholeiitic (i.e. sub-alkaline) suites are also present. Thorpe (1977) concluded that the LTVF is a geographically separate and petrologically distinct area where alkaline magmas have risen along fractures related to the Gulf of Mexico, although he attributed the ultimate origin of this volcanism to subduction of the Cocos plate. Other authors (Robin 1976, 1982b; Robin and Tournon 1978; Cantagrel and Robin 1979) proposed that the LTVF is part of the EAP related to the extension along the Gulf of Mexico coast.

More recently, Nelson and Gonzalez-Caver (1992) published new K–Ar dates along with chemical analyses of lavas from the LTVF. Verma et al. (1993) reported petrographic and major element data on rocks from this field and emphasized the significantly more basic as well as alkaline character of these rocks, as compared to the MVB rocks. Nelson et al. (1995) presented a detailed petrological study to support a conclusion similar to the one reached by Verma and Nelson (1989) for the northwestern part of the MVB, according to which alkaline magmas were derived from the underlying mantle, whereas sub-alkaline basaltic and differentiated lavas apparently showed involvement of subduction fluids and the continental crust. Finally, Verma (2002) argued from a geochemical database for basic rocks from Mexico, Central America, and several well-known rifts, many of which, especially the African ones, have no documented subduction regime in their geological history, that in southern Mexico including the LTVF, basic volcanism related to the subduction of the Cocos plate is absent, as opposed to Central America (CAVA) where the relationship of volcanism with this oceanic plate is clearly established.

Thus, a controversy regarding the origin of volcanism in the LTVF still exists. New major and trace elements and isotopic data along with the published information are used in this paper to constrain the petrogenesis of lavas in the LTVF and to support an essentially extension-related origin, with no requirement for the involvement of subduction fluids or slab melts. Furthermore, a garnet-bearing source with incompatible element enrichment is most suited to explain the trace element characteristics of these primitive magmas.

Geology of LTVF volcanics, samples, and analytical details

Detailed geology was reported by Nelson and Gonzalez-Caver (1992), Verma et al. (1993), and Nelson et al. (1995), from which the present synthesis is prepared. The LTVF is a mountainous area consisting of a NW-trending ridge about 80 km long, and covers an area of approximately 2,200 km^2 with an estimated volume of 800 km^3. The LTVF rocks can be separated into a younger and an older volcanic series. The latter covers the areas to the east and south of Laguna Catemaco (differentiated and sub-alkaline rocks from 3.3 to 1.0 Ma) as well as an elliptical area surrounding Volcán San Martín represented by basanite and alkali basalt having ages from 6.9 to 2.2 Ma (detailed map not shown to comply with space limitations; for maps see the references cited above in this section). The younger volcanic series is found in the area immediately surrounding the historic Volcán San Martín, and consists of basanite and alkali basalt of age from 0.8 Ma to the historic eruptions of 1664 and 1793 A.D. from this volcano. This volcano is a major eruptive centre for these younger series lavas. More than 250 cinder cones and maars occur on the flanks of this volcano and show local alignment of N55W, nearly parallel to the major structures in the area. According to Nelson et al. (1995) this suggests an extensional stress field in the crust beneath the LTVF.

Petrographically, all LTVF rocks contain phenocrysts and microphenocrysts of olivine, pyroxene, plagioclase, and opaque minerals, with the exception of a few samples, in which either olivine or plagioclase phenocryst is absent. Detailed petrographic description can be found in Nelson and Gonzalez-Caver (1992), Verma et al. (1993), and Nelson et al. (1995). Several pieces from the interiors of large (200–300 mm size) blocks were crushed in a hardened, pure iron container to obtain representative powders (finely ground to < 200 mesh) for chemical and isotopic analyses.

Major elements were determined by X-ray fluorescence spectrometry (XRF) at Universität Mainz, Germany, using fused glass discs (analytical details are given by Verma et al. 1992). Magma and rock types were inferred automatically according to total alkalis versus silica diagram (Le Bas et al. 1986; Le Bas 2000) and CIPW norms on an anhydrous 100% adjusted basis with Fe_2O_3/FeO ratio depending on the rock type after Middlemost (1989), using the SINCLAS computer program (Verma et al. 2002).

Trace elements (Ba to Co) were obtained by XRF at Universität Mainz, Germany, using pressed powder pallets (Verma et al. 1992) and the REE (La to Lu) by high-performance liquid chromatography (HPLC; Verma 1991) at Max-Planck-Institut für Chemie, Mainz, Germany. The analytical errors (precision and accuracy or trueness estimates) reported in these papers (Verma 1991; Verma et al. 1992) are generally between 0.5 and 2, 1 and 10, and 5 and 20% for major, trace, and REE determinations, respectively.

Radiogenic isotopes were analysed on two fully automated triple- (for Nd and Pb) and multi-collector (for Sr) MAT 261 mass spectrometers (Verma 1992) at Max-Planck-Institut für Chemie, Mainz, Germany. The $^{87}Sr/^{86}Sr$ ratios were normalized to $^{86}Sr/^{88}Sr = 0.11940$ and adjusted to SRM987 $^{87}Sr/^{86}Sr$ ratio of 0.710230. The measured $^{87}Sr/^{86}Sr$ ratio for the SRM987 standard during

the period of measurements of this study was 0.710216 ± 0.000011 (1 s; $n = 36$). The $^{143}Nd/^{144}Nd$ ratios were normalized to $^{146}Nd/^{144}Nd = 0.72190$ and adjusted to La Jolla $^{143}Nd/^{144}Nd$ ratio of 0.511860. The measured $^{143}Nd/^{144}Nd$ ratio for the La Jolla standard was 0.511833 ± 0.000012 (1 s; $n = 82$) during the same period of measurement as the LTVF samples. $\varepsilon_{Nd} = \{[(^{143}Nd/^{144}Nd)_m/(^{143}Nd/^{144}Nd)_{CHUR}] - 1\} \times 10^4$ (DePaolo and Wasserburg 1976), using $(^{143}Nd/^{144}Nd)_{CHUR} = 0.512638$. Further, the errors for individual Sr and Nd isotope ratios are two times the standard error of the mean ($2s_E$). For the Pb isotopes, 40–50 ratios were collected and the fractionation correction was applied using SRM982 standard. Age correction on Sr and Nd isotopic ratios (from this paper as well as from Nelson et al. 1995) was carried out using known or assumed age data (inferred from the geologic map of Nelson et al. 1995 and sample locations) and measured Rb, Sr, Sm, and Nd concentrations; for samples with no available concentration data, assumed values (Rb/Sr of 0.02 and Sm/Nd of 0.2) were used. Note that the age corrections are generally well within the experimental errors on measured Sr and Nd isotopic ratios and, therefore, the uncertainties in actual ages and trace element concentrations are not really important.

Databases

New results of major elements and Sr and Nd isotopic ratios for 16 LTVF samples are presented in Table 1, whereas trace element data including rare-earth elements (REE) and Pb isotopic ratios for three selected samples are given in Table 2. Unfortunately, no Pb concentration data are still available for LTVF rocks. The database for the LTVF area was established from these data and all published sources (Nelson and Gonzalez-Caver 1992; Verma et al. 1993; Nelson et al. 1995; Verma 2002).

To better understand the volcanism of the LTVF, a comprehensive compilation of geochemical data from well-known rifts and extension-related areas as well as continental break-up regions was considered necessary. The rifts represented in this database are: Rio Grande, USA (Johnson and Lipman 1988; Duncker et al. 1991; Gibson et al. 1992; McMillan et al. 2000); Abu Gabra (Davidson and Wilson 1989); East Africa (Aoki et al. 1985; De Mulder et al. 1986; Auchapt et al. 1987; Class et al. 1994); Ethiopia (Barberi et al. 1975; Hart et al. 1989; Trua et al. 1999; Deniel et al. 1994; Barrat et al. 2003); Gregory (Macdonald et al. 1995); and Kenya (Bell and Peterson 1991; Le Roex et al. 2001; Macdonald et al. 2001). Similarly, the extension-related or intraplate-type volcanic fields are: Basin and Range, USA (Singer and Kudo 1986; Lum et al. 1989; Moyer and Esperança 1989; Perry et al. 1990; Fitton et al. 1991); Hurricane volcanic field, Utah (Smith et al. 1999); Western USA (Kempton et al. 1991); San Quintín volcanic field, Baja California, Mexico (Rogers et al. 1985; Saunders et al. 1987; Storey et al. 1989; Luhr et al. 1995); Massif Central, France (Chauvel and Jahn 1984); Saudi Arabia (Camp et al. 1991); Taiwan strait (Chung et al. 1994); northwestern Taiwan (Chung et al. 1995); Eastern China (Peng et al. 1986; Zhi et al. 1990; Basu et al. 1991; Fan and Hooper 1991; Liu et al. 1994); NE China (Liu et al. 1992; Zhang et al. 1995; Hsu et al. 2000); N China (Han et al. 1999); and SE China (Zou et al. 2000). Eastern and NE parts of China have been referred to as either a rift (Liu et al. 1994; Hsu et al. 2000) or an extension-related area (Fan and Hooper 1991; Liu et al. 1992). Finally, the continental break-up regions are represented by basalts from: Antarctica (Brewer et al. 1992); Paraná (Hawkesworth and Gallagher 1992; Peate and Hawkesworth 1996); Columbia River (Hooper 1988); Wrangellia (Lassiter et al. 1995); Greenland (Holm et al. 1992); Karoo (Duncan et al. 1984; Marsh 1987); Kwanza (Marzoli et al. 1999); Seychelles (Devey and Stephens 1992); and Deccan (Peng et al. 1994; Melluso et al. 1995). Complete data sets mainly for basic rocks from these rifts and extension-related areas as well as continental break-up regions were compiled in this database. Although the continental break-up regions were compiled in the same database, their separate identity was maintained in different diagrams constructed for comparison purposes.

Similarly, an extensive compilation of data for island and continental arcs, including the CAVA, was also established. The island arcs represented in this database are: Aleutian (Kay et al. 1982; Brophy 1986; Nye and Reid 1986; Romick et al. 1990; Singer et al. 1992; Kay and Kay 1994; Myers et al. 1985, 2002); Burma (Stephenson and Marshall 1984); Izu-Bonin (Tatsumi et al. 1992; Taylor and Nesbitt 1998); Japan (Sakuyama and Nesbitt 1986; Togashi et al. 1992; Edwards et al. 1994; Tamura 1994; Kita et al. 2001); Kamchatka (Kepezhinskas et al. 1997); Kuril (Zhuravlev et al. 1987; Nakagawa et al. 2002); Lesser Antilles (Arculus 1976; Brown et al. 1977; Thirlwall and Graham 1984; Devine 1995; Smith et al. 1996; Thirlwall et al. 1997; Defant et al. 2001); Luzon (Defant et al. 1991a); Mariana (Hole et al. 1984; Woodhead 1988; Bloomer et al. 1989; Elliott et al. 1997); New Britain (Woodhead and Johnson 1993); New Hebrides (Dupuy et al. 1982); Papua-New Guinea (Hegner and Smith 1992); Philippines (Knittel et al. 1997; Defant et al. 1989; Bau and Knittel 1993); Sangihe (Tatsumi et al. 1991); South Shetland (Smellie 1983); Sunda-Banda (Whitford et al. 1979; Foden and Varne 1980; Wheller et al. 1987; Stolz et al. 1988, 1990; Hoogewerff et al. 1997; Turner and Foden 2001; Turner et al. 2003); Tonga-Kermadec-New Zealand (Bryan et al. 1972; Ewart et al. 1977; Gamble et al. 1995); Vanuatu (Barsdell 1988; Barsdell and Berry 1990; Raos and Crawford 2004); and Yap arc system (Ohara et al. 2002). For the Andean continental arc, data were compiled from Deruelle (1982), Frey et al. (1984); Hickey et al. (1986), Gerlach et al. (1988), Kay et al. (1987, 1988); Hickey-Vargas et al. (1989), Stern et al. (1990), Tormey et al. (1991), and López-Escobar et al. (1993). Finally,

also included were data from the CAVA downloaded from M.J. Carr's website (http://www.rci.rutgers.edu/~carr; June 2004); only rocks from the northern part of this province were used here to restrict the comparison to a well-defined subduction-related segment of the CAVA, lying relatively close to the area of study (LTVF) and being the result of the subduction of the same oceanic plate (Cocos plate; Fig. 1).

An extensive database for the eastern part of the MVB (E-MVB; an updated version of Verma 2004) was also established from several sources (Demant 1981; Verma and Lopez 1982; Kudo et al. 1985; Negendank et al. 1985; Ferriz and Mahood 1987; Besch et al. 1995; Carrasco-Núñez 2000; Siebert and Carrasco-Núñez 2002; Gómez-Tuena et al. 2003; Verma 1983, 1984, 2000a, 2001, 2002). The easternmost part of the MVB overlaps with the EAP (Fig. 1); for this overlap region, isotope data reported by Gómez-Tuena et al. (2003) were compiled in this database. For the EAP as a whole, additional chemical data were also compiled from Robin (1976), Robin and Tournon (1978), Nick (1988), Morton-Bermea (1990), Orozco-Esquivel (1995), Ramírez-Fernández (1996), and Treviño-Cázares et al. (2005). No radiogenic isotope data for the EAP were available in any of these papers. A compilation of Mexican lower crust compositions was also accomplished from several sources (Patchett and Ruiz 1987; Ruiz et al. 1988a, b; Roberts and Ruiz 1989; Heinrich and Besch 1992; Schaaf et al. 1994). Similarly, altered basalt and sediment data from the Cocos plate (to represent the downgoing slab) were also added to this database from an earlier compilation by Verma (2000b).

Results

All LTVF rocks analysed in this study as well as from the published literature are plotted in a total alkali–silica (TAS) diagram (Le Bas et al. 1986; Le Bas 2000; Fig. 2a) and are compared with rocks from two Mexican volcanic provinces (EAP and E-MVB; Fig. 2b), from representative rifts or extension-related areas (Rio Grande, western USA, Hurricane volcanic field, Djibouti, and China; Fig. 2c, d) as well as with the CAVA rocks plotted here as representative of arcs (Fig. 2e) and the Andean continental arc (Fig. 2f). The LTVF rocks (50 samples plotted in Fig. 2a) are mostly ultrabasic (15 samples) and basic (26 samples) alkaline rocks, with only a few sub-alkaline (4 samples: 1 basic and 3 intermediate rocks) and differentiated rocks (5 samples). Surprisingly, the LTVF rocks show widely varying total alkali contents at any given SiO_2 level (Fig. 2a), which is also the case of two other Mexican areas (EAP and E-MVB; Fig. 2b), especially the EAP, as well as of numerous rifts (Fig. 2c, d). The major element compositions of the CAVA (Fig. 2e) and Andean continental arc rocks (Fig. 2f), on the other hand, show a well-defined evolution, mainly in the sub-alkaline field, from sub-alkali basalt to rhyolite (rhyolitic rocks are not shown), except for some alkaline rocks, mostly from the back-arc region.

Harker-type diagrams (plots not shown) show, with increasing SiO_2, decreasing TiO_2, MgO, Mg#, and to a lesser extent, P_2O_5, but less regular trends for Al_2O_3 (although somewhat increasing with SiO_2) and K_2O. The REE in LTVF rocks show light REE (LREE)-enriched, heavy REE(HREE)-depleted patterns (only a few representative primitive samples from the LTVF database are shown in Fig. 3). The REE patterns of differentiated rocks (plots not shown) are also LREE-enriched but show rather flat HREE (see Nelson et al. 1995 for more details).

A few representative LTVF primitive rocks (for definition see below the section of Heterogeneous mantle melting) are also plotted on a primitive mantle-normalized multi-element diagram (Fig. 4a) and compared with similar primitive rocks from the EAP and E-MVB (Fig. 4b), continental rifts (Fig. 4c), and continental arcs (Fig. 4d). The LTVF rocks show a highly significant enrichment of Th and U with respect to (w.r.t.) Rb and Ba, and a depletion of Nb and Ta w.r.t. Th and U (but much less pronounced depletion of Nb and Ta w.r.t. Rb and Ba or w.r.t. K and La; Fig. 4a). Trachybasaltic magmas from the EAP and E-MVB also show this behaviour (Fig. 4b). The Th–U enrichment w.r.t. Rb–Ba is not a common feature of continental rifts (although the Rio Grande basanite does show Th enrichment; Fig. 4c) nor is the case of island and continental arcs (in the CAVA and Andes, Ba is the most enriched element of the group of Rb–Ba–Th–U; Fig. 4d). Furthermore, basic magmas from the front-arc (of the CAVA and Andes) are significantly depleted in Nb w.r.t. Ba, but those from the back-arc are significantly enriched showing a positive Nb anomaly (Fig. 4d).

The Sr, Nd, and Pb isotopic ratios for the LTVF magmas range as follows: $^{87}Sr/^{86}Sr$ 0.70300–0.70420; $^{143}Nd/^{144}Nd$ 0.51271–0.51310; $^{206}Pb/^{204}Pb$ 18.62–18.92; $^{207}Pb/^{204}Pb$ 15.47–15.65; $^{208}Pb/^{204}Pb$ 38.06–38.64. Although these isotopic ratios of primitive and evolved rocks show overlapping ranges, the Sr isotope ratios of primitive rocks from the LTVF (0.70300–0.70379; mean $\pm$ 1 s $\sim 0.70336 \pm 0.00016$; 28 data) are slightly lower than those for evolved rocks (0.70326–0.70418; $\sim 0.70356 \pm 0.00030$; 7 data), and the corresponding Nd isotopes are slightly higher ($\sim 0.51292 \pm 0.00006$ for primitive vs. $\sim 0.51287 \pm 0.00009$ for evolved rocks). On a Sr–Nd isotope diagram (Fig. 5a), the LTVF primitive rocks [Mg-value > 63; $(SiO_2)_{adj} < 52\%$] plot in the same field as the primitive rocks from continental rifts and extension-related areas as well as island and continental arcs. A similar comparison of these LTVF rocks is presented with the E-MVB (and the overlap region of the EAP and E-MVB) primitive rocks as well as with the Mexican lower crust (Fig. 5b). Altered basalts and sediments from subducting Cocos plate ("Downgoing slab" in Fig. 5a, b) are included to show that the slab composition (basalt–sediment mixing curve) plots considerably to the right of the LTVF and E-MVB

Table 1 New major element, CIPW norm, and isotopic data for 16 volcanic rock samples from the LTVF, Mexico

Sample	TUX04	TUX07	TUX15	TUX06	TUX01	TUX02	TUX05	TUX13
Long. (°W)	95.07056	95.09333	95.29306	95.09139	95.09750	95.03333	95.07222	95.26361
Lat. (°N)	18.57972	18.64389	18.46500	18.62500	18.42389	18.51361	18.59722	18.43861
Age (Ma)	~7	~7	~2.6	~7	~1.6	~0.8	~7	~2.6
Rock-type	BSN, mnp	BSN, mnp	BSN, mnp	BSN, bsn	B, alk	B, alk	B, alk	B, alk
Magma-type	Ultrabasic	Ultrabasic	Ultrabasic	Ultrabasic	Basic	Basic	Basic	Basic
SiO_2	41.78	42.46	42.89	44.43	44.60	45.82	45.59	45.92
TiO_2	2.64	1.83	2.30	1.94	1.80	1.89	1.66	1.64
Al_2O_3	11.70	11.86	12.21	12.33	11.77	12.59	13.05	12.21
$Fe_2O_3^T$	13.90	12.61	13.08	12.71	11.52	11.63	11.37	11.47
MnO	0.19	0.20	0.19	0.20	0.18	0.17	0.19	0.17
MgO	13.28	14.34	13.65	12.96	14.11	13.07	11.93	14.12
CaO	11.04	12.72	11.07	11.20	10.79	11.01	12.00	10.53
Na_2O	3.92	2.78	3.47	2.68	2.73	2.65	2.28	2.58
K_2O	1.74	0.69	1.43	0.77	0.80	0.94	1.05	0.82
P_2O_5	0.84	0.80	0.75	0.78	0.82	0.47	0.36	0.53
LOI	−0.30	0.00	−0.34	0.12	0.18	0.00	0.27	0.00
Sum	100.73	100.29	100.70	99.12	99.30	100.24	99.75	99.99
$(SiO_2)_{adj}$	41.84	42.79	42.92	44.35	45.44	46.16	46.28	46.38
$(Na_2O + K_2O)_{adj}$	5.67	3.50	4.90	3.52	3.60	3.62	3.38	3.43
Q	–	–	–	–	–	–	–	–
Or	–	4.11	7.78	4.64	4.82	5.60	6.30	4.89
Ab	–	0.02	–	9.24	12.21	12.71	10.13	14.51
An	9.20	17.98	13.53	19.75	17.83	19.83	22.61	19.50
Lc	8.07	–	0.53	–	–	–	–	–
Ne	18.00	12.84	15.92	7.54	6.14	5.35	5.12	4.09
Di	31.46	32.42	29.35	25.61	25.06	25.79	28.53	23.87
Hy	–	–	–	–	–	–	–	–
Ol	22.88	24.45	23.88	24.74	25.93	23.42	20.71	26.19
Mt	3.08	2.81	2.89	2.87	2.60	2.59	2.55	2.56
Il	5.02	3.50	4.37	3.76	3.48	3.62	3.20	3.14
Ap	1.95	1.87	1.75	1.84	1.94	1.10	0.85	1.24
Cs	0.34	–	–	–	–	–	–	–
Mg#	69.07	72.66	70.92	70.44	74.11	72.43	71.04	74.21
FeO^T/MgO	0.94	0.79	0.86	0.88	0.74	0.80	0.86	0.73
$^{87}Sr/^{86}Sr \pm (2s_E)$	0.703236 ± 0.000014	0.703488 ± 0.000013	0.703297 ± 0.000013	0.703380 ± 0.000008	0.703384 ± 0.000008	0.703344 ± 0.000006	0.703599 ± 0.000008	0.703458 ± 0.000011
$^{143}Nd/^{144}Nd \pm (2s_E)$	0.512940 ± 0.000012	0.512941 ± 0.000014	0.512956 ± 0.000014	0.512936 ± 0.000008	0.512938 ± 0.000008	0.512949 ± 0.000013	0.512911 ± 0.000013	0.512950 ± 0.000008
$(^{87}Sr/^{86}Sr)_i$	0.703227	0.703482	0.703294	0.703374	0.703383	0.703343	0.703593	0.703456
$(^{143}Nd/^{144}Nd)_i$	0.512934	0.512935	0.512954	0.512930	0.512937	0.512948	0.512905	0.512948
$(\varepsilon_{Nd})_i$	5.78	5.80	6.16	5.70	5.83	6.05	5.22	6.05

The subscript 'adj' refers to adjusted data (anhydrous 100% adjusted basis); $Mg\# = 100Mg^{2+}/(Mg^{2+} + Fe^{2+})$, atomic; $Fe_2O_3^T$ = total from the "Data repository" of Verma (2002). Complete duplicate analysis of TUX03 shows the reproducibility of major elements for the 2002) *BSN, mnp*: basanite, melanephelinite; *BSN, bsn*: basanite; *B, alk*: alkali basalt; *PIC*: picrite; *BA*: basaltic andesite; ($2s_E$): two times

rocks. Similarly, on other isotope–isotope diagrams (Fig. 6a–d), the LTVF primitive rocks are plotted along with those from the E-MVB. The "Downgoing slab" basalt–sediment mixing curve indicates that the LTVF and E-MVB rocks fall close to this curve at ~1–5% sediment with 99–95% altered basalt mixture [$^{87}Sr/^{86}Sr$ vs. $^{206}Pb/^{204}Pb$ (Fig. 6a) and $^{208}Pb/^{204}Pb$ vs. $^{206}Pb/^{204}Pb$ (Fig. 6d)], but at ~5–30% sediment with 95–70% altered basalt mixture [$^{143}Nd/^{144}Nd$ vs. $^{206}Pb/^{204}Pb$ (Fig. 6b)] and mostly away from this mixing curve on $^{207}Pb/^{204}Pb$ vs. $^{206}Pb/^{204}Pb$ diagram (Fig. 6c). Additional isotope data available for seamounts from the Cocos plate (e.g. Zindler et al. 1984; Graham et al. 1988; Werner et al. 2003) were not included in Fig. 6 because the corresponding locations do not represent the downgoing slab. Low-temperature seawater alteration of basaltic rocks is a common process to significantly modify the chemistry of downgoing slabs, including Sr, Pb, and, to a lesser extent, Nd isotope ratios, as compared to the younger parts of the oceanic plates (e.g. Verma 1992; Jochum and Verma 1996, and references therein).

Bivariate diagrams based on carefully selected variables (Fig. 7a–f) were constructed using trace elements and their ratios in only primitive rocks from the present database of the LTVF, continental rifts, extension-related areas, continental break-up regions, island arcs, the CAVA, and the Andes. These chosen variables are excellent geochemical fingerprints of subducted slab and mantle sources. Similar combinations of elements were used in bivariate diagrams by Nelson et al. (1995), in which primitive as well as differentiated rocks from

Table 1 (Contd.)

TUX16	TUX10	TUX03-a	TUX03-b	TUX09	TUX08	TUX14	TUX11
95.30833	95.01306	95.05972	95.05972	95.01917	95.04528	95.29611	95.01500
18.53528	18.40722	18.53111	18.53111	18.43111	18.43639	18.45944	18.36806
~2.6	~1.6	~0.8	~0.8	~1.6	~1.6	~2.6	~1.6
B, alk	B, alk	B, alk	B, alk	B, alk	B, alk	PIC	BA
Basic	Basic	Basic	Basic	Basic	Basic	Basic	Intermediate
46.19	46.02	46.02	46.64	46.26	46.80	43.94	54.54
1.42	1.32	1.86	1.86	1.36	1.67	1.50	1.00
13.25	14.16	12.95	13.09	14.38	13.02	11.52	18.18
10.94	11.18	11.35	11.04	11.85	11.01	11.00	8.32
0.18	0.19	0.18	0.18	0.18	0.18	0.18	0.15
13.57	11.49	12.22	12.08	11.67	12.22	15.81	3.74
10.76	11.08	10.96	11.02	11.95	10.87	11.19	9.94
2.76	2.63	2.67	2.76	3.02	2.68	2.03	3.74
0.78	0.84	0.90	0.93	0.68	0.89	0.73	1.24
0.33	0.55	0.49	0.41	0.33	0.52	0.46	0.26
0.00	0.08	0.00	0.00	−0.74	0.06	1.38	0.42
100.18	99.54	99.60	100.01	100.94	99.92	99.74	99.53
46.54	46.72	46.66	47.08	45.95	47.31	45.10	54.38
3.57	3.52	3.62	3.72	3.68	3.61	2.83	5.06
–	–	–	–	–	–	–	2.35
4.64	5.04	5.39	5.55	3.99	5.32	4.43	7.44
13.43	15.59	15.06	15.59	10.90	17.26	7.91	32.15
21.62	24.72	20.98	20.77	23.51	21.09	20.70	29.61
–	–	–	–	–	–	–	–
5.47	3.79	4.25	4.33	7.84	3.07	5.27	–
24.06	22.13	24.85	25.48	26.84	24.10	26.55	11.28
–	–	–	–	–	–	–	12.02
24.84	22.38	22.19	21.30	20.98	22.27	28.64	–
2.44	2.51	2.54	2.46	2.60	2.46	2.50	2.60
2.72	2.54	3.58	3.56	2.57	3.21	2.92	1.93
0.77	1.29	1.15	0.96	0.76	1.22	1.09	0.61
–	–	–	–	–	–	–	–
74.35	70.61	71.56	71.89	69.71	72.18	77.06	53.07
0.72	0.88	0.84	0.82	0.91	0.81	0.63	2.00
0.703388 ± 0.000013	0.703512 ± 0.000006	0.703374 ± 0.000008		0.703403 ± 0.000008	0.703388 ± 0.000007	0.703527 ± 0.000013	0.703444 ± 0.000008
0.512967 ± 0.000008	0.512945 ± 0.000014	0.512936 ± 0.000008		0.512942 ± 0.000012	0.512933 ± 0.000012	0.512902 ± 0.000015	0.512880 ± 0.000010
0.703386	0.703511	0.703373		0.703402	0.703387	0.703525	0.703443
0.512965	0.512944	0.512935		0.512941	0.512932	0.512900	0.512879
6.38	5.96	5.80		5.90	5.73	5.11	4.70

iron expressed as Fe_2O_3; FeO^T = total iron expressed as FeO. Data for two samples (TUX04 and TUX15) in this table and Table 2 are entire analytical process (sample crushing, glass bead preparation, and XRF counting). Rock-type abbreviations are (also see Verma et al. the standard error of the mean for the isotopic data

the LTVF were plotted to show the effects of crustal contamination.

As an example, a high Ba/Nb ratio [Ba, a large ion lithophile element (LILE), is fluid mobile and therefore, indicative of slab; and Nb, a high field strength element (HFSE), is relatively fluid immobile and, therefore, indicative of mantle wedge] is considered an excellent subduction signal. Similarly, a high Sr/P ratio (Sr, a LILE, is fluid mobile, indicative of slab; and P, a HFSE, is fluid immobile, indicative of mantle) is also an excellent subduction signal (e.g. Davidson 1996; Borg et al. 1997). On the contrary, low Ba/Nb and Sr/P ratios are indicators of mantle sources without a significant subduction component and/or crustal contamination. These ratios are low (Ba/Nb < 30; Sr/P < 0.5) in the LTVF primitive rocks (Fig. 7a), as is the case of most such rocks from continental rifts, extensional regions, and break-up areas. The LTVF primitive rocks contrast from similar rocks from island and continental arcs including the CAVA. Most of the arc rocks plot outside the LTVF field because they show significantly higher values of either or both of these parameters. A plot of Rb/La and Cs/Th (Fig. 7b) also shows low values of both ratios for the LTVF and rift rocks, with high values of both ratios being indicative of subduction signal as exemplified by most arc rocks. Note that although the data for Cs/Th are scarce, its high values are typical of arcs.

$[Nb/Nb^*_1]_{Primitive\text{-}mantle}$ anomaly is a good quantitative measure of Nb depletion (value < 1) or enrichment (value > 1) w.r.t. Th and K as compared to the primitive mantle. A plot of this parameter against the slab-indicative parameter Ba/La (Fig. 7c) shows that the LTVF

Table 2 New trace element and Pb isotope data for three selected samples from the LTVF, Mexico

Sample	TUX04, BSN, mnp	TUX15, BSN, mnp	TUX09, B, alk
Ba	536	414	248
Nb	71	43.7	13.4
Zr	282	222	115.6
Y	27.8	24.2	20.3
Sr	1,008	931	582.2
Rb	33.1	24.8	10.7
Zn	133	106	82
Cu	80	83	96
Ni	330	333	220
Cr	640	658	606
V	281	245	289
Co	76	56	53
La	56	56	23.8
Ce	109	107	48
Pr	12.8	12.1	5.7
Nd	51.6	50.6	24.4
Sm	10.2	9.7	4.98
Eu	3.05	2.75	1.51
Gd	8.6	8.0	4.76
Tb	1.26	1.10	0.6
Ho	0.89	0.82	0.73
Er	2.05	1.92	1.92
Tm	0.22	0.18	0.25
Yb	1.40	1.21	1.68
Lu	0.20	0.16	0.20
$^{206}Pb/^{204}Pb \pm (2s_E)$	18.922 ± 0.004	18.826 ± 0.005	18.743 ± 0.004
$^{207}Pb/^{204}Pb \pm (2s_E)$	15.607 ± 0.005	15.574 ± 0.004	15.592 ± 0.004
$^{208}Pb/^{204}Pb \pm (2s_E)$	38.644 ± 0.008	38.517 ± 0.007	38.475 ± 0.008

primitive rocks have low Ba/La (< 14) and relatively high $[Nb/Nb^*_1]_{Primitive\text{-}mantle}$ (> 0.28). The value of this Nb anomaly parameter, although showing Nb depletion, is much higher than most arc values, which are as low as ~0.05. Furthermore, because of Th enrichment, i.e. because of high Th concentrations, and not due to low Nb concentrations as indicated below in Fig. 7d, the LTVF rocks show lower $[Nb/Nb^*_1]_{Primitive\text{-}mantle}$ than most continental rift rocks (Fig. 7c).

A plot of $[Nb/Nb^*_2]_{Primitive\text{-}mantle}$ anomaly (defined w.r.t. Ba and La) against Nb concentration (Fig. 7d) shows that the LTVF rocks have Nb > 12 ppm and $[Nb/Nb^*_2]_{Primitive\text{-}mantle} > 0.3$, and occupy a field similar to the compiled rifts and extension-related areas, but distinct from island and continental arcs. Note numerous primitive samples from rifts have similar values for these parameters, in particular $[Nb/Nb^*_2]_{Primitive\text{-}mantle} < 1$; in fact, some of them even show $[Nb/Nb^*_2]_{Primitive\text{-}mantle} < 0.3$ (Fig. 7d). Some rift and back-arc rocks do show a positive Nb anomaly ($[Nb/Nb^*_2]_{Primitive\text{-}mantle} > 1$). I propose that Nb depletion with respect to Ba and La (i.e. $[Nb/Nb^*_2]_{Primitive\text{-}mantle} < 1$) must be accompanied by low Nb concentration (< 10 ppm) in primitive rocks for such a depletion to be a diagnostic feature of an arc environment (Fig. 7d). Likewise, high Zr/Nb combined with low Zr concentration (< 110 ppm) in primitive rocks seems to be a similar diagnostic feature for arcs (plot not shown).

The La/Yb ratio [La, a light REE (LREE), is a highly incompatible element, and Yb, a heavy REE (HREE), is a less incompatible element; both are relatively fluid-immobile elements] is an excellent indicator of degree of enrichment (high value of La/Yb for enriched sources) or degree of melting (lower value of La/Yb for higher degree of melting) of mantle sources (Verma 2002). Similarly, the La/Sm ratio is also an indicator of mantle sources and their degree of melting. In La/Yb–La/Sm diagram (Fig. 7e) the LTVF primitive rocks and most rift rocks show high values of both parameters, with very few rocks from arcs falling in the LTVF field.

Finally, high values of both $LILE_E/LREE_E$ and $LILE_E/HFSE_E$ ratios (LILE showing combined or averaged behaviour of K, Rb, Ba, and Sr; LREE representing La, Ce, and Nd; and HFSE representing Ti, P, Zr, and Nb; the subscript E refers to silicate earth normalization; see Fig. 7 for explanation) are excellent subduction signals (Verma 2004). These ratios are low in the LTVF magmas, as is the case of most rifts and extension-related areas (Fig. 7f; see explanation of Fig. 7 for the method of calculations). On the other hand, both ratios are typically very high for primitive rocks from arcs (for most of them $[LILE_E/LREE_E] \approx 1.5–5.0$; and $[LILE_E/HFSE_E] \approx 2.8–10$).

It should be noted that a few back-arc rocks such as those from Yohoa volcano in CAVA (Fig. 1), but *not* many other, plot in the fields outlined for the LTVF and rift rocks (Fig. 7). In summary, in terms of these parameters the characteristics of the LTVF primitive rocks (Fig. 7; and this database) can be summarized as follows: Ba/Nb < 30; Sr/P < 0.5; Rb/La < 1.3; Cs/Th < 0.25; $[Nb/Nb^*_1]_{Primitive\text{-}mantle} > 0.28$; Ba/La < 14; $[Nb/Nb^*_2]_{Primitive\text{-}mantle} > 0.3$; Nb > 12 ppm; Zr/Nb < 12; Zr > 110 ppm; $[La/Yb]_{ChN} > 9$; $[La/Sm]_N > 2.6$; $[LILE_E/LREE_E] < 1.5$; and $[LILE_E/HFSE_E] < 2.8$. Any petrogenetic model should explain these "rift-like" chemical characteristics of the LTVF and their significant differences from "arc-type" chemistry.

Discussion

Rock types and their distribution

No rocks with > 60% SiO_2 have yet been reported from the LTVF (Fig. 2a). This contrasts with the neighbouring northern part of the CAVA province (volcanoes in Guatemala, El Salvador, Honduras, Nicaragua, and northwestern part of Costa Rica; Fig. 2e; e.g. Carr et al. 1982), where differentiated high-silica dacitic and rhyolitic rocks are commonly present.

Furthermore, the distribution of rock types shown by the LTVF (Fig. 2a) is typical of many well-known rifts and extension-related areas (some selected regions are shown in Fig. 2c, d) including the Mexican EAP and the E-MVB (LTVF and EAP are more similar in this respect; Fig. 2b), but differs significantly from that observed in arcs compiled in the present study

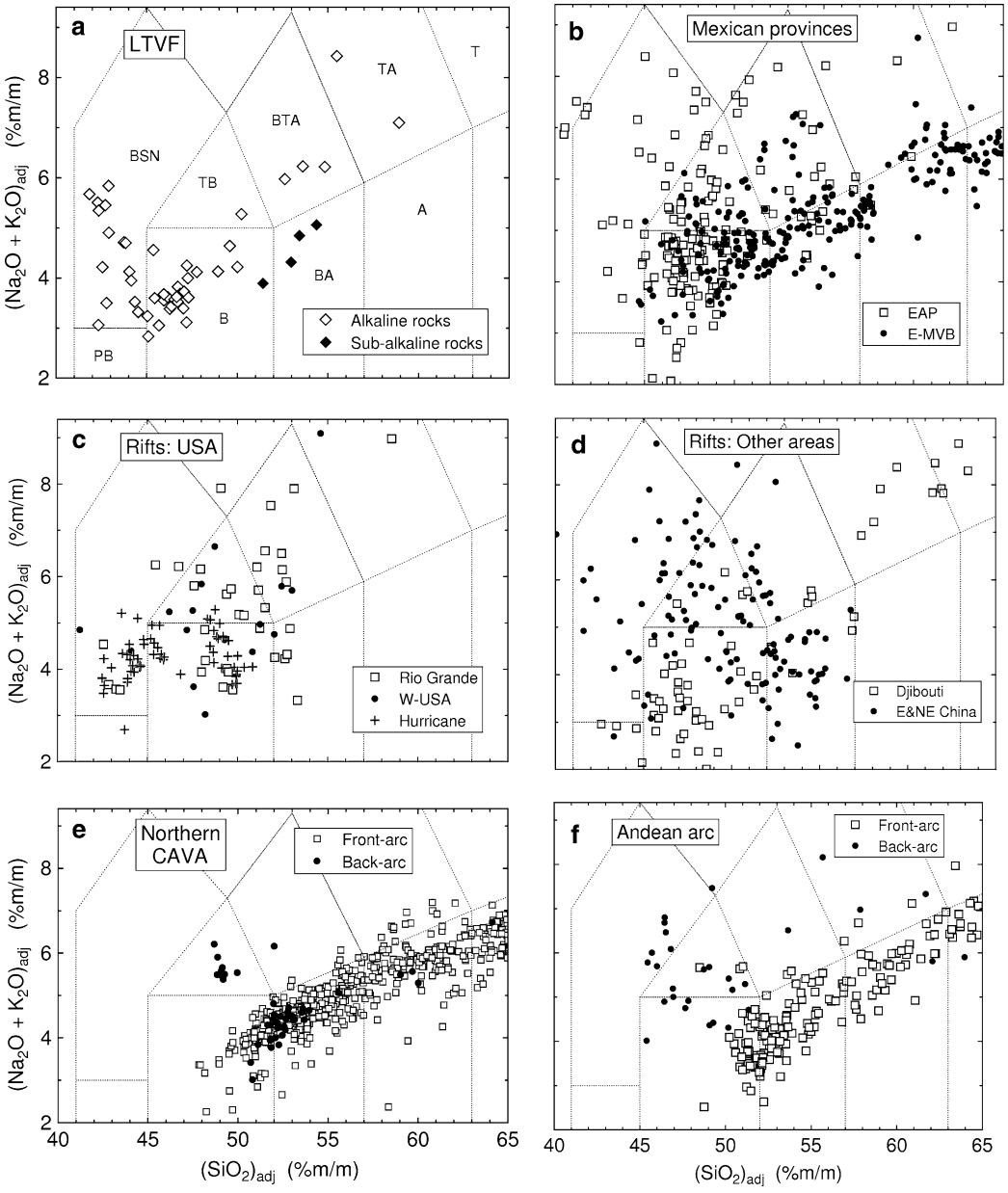

Fig. 2 A total alkali–silica (TAS) classification diagram for rocks from the Los Tuxtlas volcanic field (LTVF), the Eastern Alkaline Province (EAP), the eastern part of the Mexican Volcanic Belt (E-MVB; east of the 97°W), well-known rifts, CAVA, and the Andes. Major element concentration data are on an anhydrous 100% adjusted basis and expressed in %m/m (mass/mass unit; this unit name is now recommended to be used instead of the more conventional wt%). The rock-type fields are: *BSN* basanite, *PB* picrobasalt, *B* basalt, *TB* trachybasalt, *BTA* basaltic trachyandesite; *BA* basaltic andesite; *TA* trachyandesite, *A* andesite, *T* trachyte. **a** LTVF (alkaline and sub-alkaline rocks are distinguished); **b** extension-related Mexican provinces (EAP and E-MVB); **c** rifts from USA (Rio Grande, Western USA, and Hurrican volcanic field); **d** rifts or extension-related areas from Africa (Djibouti) and China (East and North-East China); **e** subduction-related volcanic rocks from the northern part of the CAVA (front-arc and back-arc rocks are distinguished); and **f** subduction-related volcanic rocks from the Andean continental arc (also front-arc and back-arc rocks are distinguished)

(Fig. 2e, f). In continental arcs, ultrabasic rocks are practically absent and basic rocks are scarce being much less abundant than intermediate and felsic rocks (for the CAVA, see Fig. 2e and http://www.rci.rutgers.edu/~carr; for the Andes, see Fig. 2f, see also papers by Deruelle 1982; Hickey et al. 1986; Kay et al. 1987, 1988; Gerlach et al. 1988; Tormey et al. 1991; López-Escobar et al. 1993; Kay and Gordillo 1994). Therefore, if, as suggested by Thorpe (1977) and Nelson et al. (1995), the LTVF were a continental arc (arc and back-arc in the same place according to Nelson et al. 1995), and, in fact, the LTVF should be an arc in the framework of the subduction of the Cocos plate beneath the North American plate (Fig. 1), the rock type distribution is certainly not typical of a continental arc.

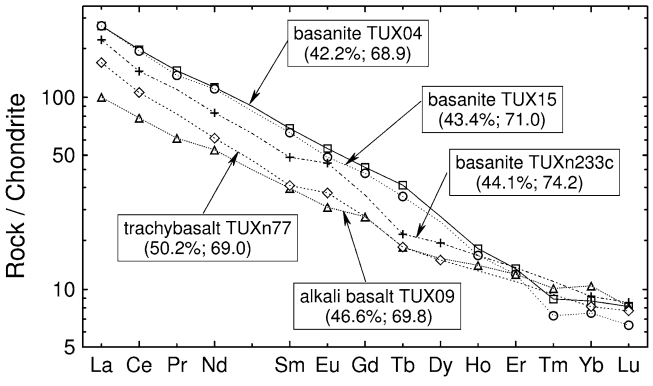

Fig. 3 Chondrite-normalized REE plots for selected primitive rocks from the LTVF [samples are identified by their names as well as $(SiO_2)_{adj}$ and Mg# in *parentheses*; the $(SiO_2)_{adj}$ parameter is the adjusted SiO_2 value from the SINCLAS program by Verma et al. 2002]. Average chondrite values (ppm or μg/g) used for normalization are from McDonough and Sun (1995): La 0.237; Ce 0.613; Pr 0.0928; Nd 0.457; Sm 0.148; Eu 0.0563; Gd 0.199; Tb 0.0361; Dy 0.246; Ho 0.546; Er 0.160; Tm 0.247; Yb 0.161; and Lu 0.0246

Isotopic constraints

Numerous primitive rocks from island and continental arcs, including the CAVA, fall in an area to the right of the mantle array, closer to the curve represented by basalt–sediment mixtures from the downgoing Cocos plate (Fig. 5a). This tendency can be explained by three- or four-component mixtures of a mantle less-depleted than MORB, a MORB mantle, and the altered MORB and sediments of respective downgoing slab (see schematics of arrows in Fig. 5a). The location of arc rocks to the right of the mantle array shows a direct link of these volcanic rocks with the subduction process (involvement of subducted slab in magma genesis either through slab melts or fluids). Sr–Nd isotopic data of the LTVF primitive rocks (Fig. 5a) plot in a wide area close to numerous rocks from rift or extension-related areas (in spite of their different histories of evolution), implying a similar tectonic origin for the LTVF. It is noteworthy that none of the LTVF rocks plots at locations right of the mantle array, near the "Downgoing slab" (Fig. 5a, b).

The combined isotopic Sr–Nd constraint (the "Sr-shift"), viz., a shift of arc magmas towards higher $^{87}Sr/^{86}Sr$ values at a given $^{143}Nd/^{144}Nd$ or a shift towards higher $^{87}Sr/^{86}Sr$ and lower $^{143}Nd/^{144}Nd$ values, i.e. for both these trends, a general shift towards the right of the "mantle array" (see island and continental arcs data in Fig. 5a), is a very strong criterion for a direct subduction relationship through involvement of dehydration fluids and/or slab melts in mantle melting. Such a shift has been observed not only in the CAVA (Feigenson and Carr 1986; Carr et al. 1990), but also in many other arcs if not all of them (although this observation was not specifically emphasized by the respective authors), such as Lesser Antilles arc (Hawkesworth et al. 1979; White and Patchett 1984; Davidson 1985, 1986; White and Dupré 1986; Smith et al. 1996; Thirlwall et al. 1997), South Sandwich island arc (Hawkesworth et al. 1977), New Britain island arc (DePaolo and Johnson 1979; White and Patchett 1984; Woodhead and Johnson 1993), Sunda arc (Hoogewerff et al. 1997), Sangihe arc (Tatsumi et al. 1991), Marianas arc (White and Patchett 1984; Lin et al. 1990), Izu-Bonin arc (Taylor and Nesbitt 1998), Kamchatka arc (Kepezhinskas 1995), Tonga-Kermadec arc (Gamble et al. 1995), and Philippines arc (Knittel et al. 1997). Further support for this proposal comes from the Franciscan subduction complex, California, where this tendency of Sr–Nd isotopic data clearly persists for metabasaltic rocks (Nelson 1995) or from leaching studies of oceanic basalts (Verma 1992).

This isotopic tendency is clearly not observed in the LTVF because the data plot within or even to the left of the "mantle array" (Fig. 5a). But if we assume the horizontal spread of the isotopic compositions of the LTVF (i.e. increase in $^{87}Sr/^{86}Sr$ at a given $^{143}Nd/^{144}Nd$ or an increase in $^{87}Sr/^{86}Sr$ accompanied by an increase in $^{143}Nd/^{144}Nd$) to have resulted from the involvement of the subducted slab, the rocks with a higher slab input should presumably lie closer to the trench and those with a lesser slab component farther away from it, towards the Gulf of Mexico coast (Fig. 1). The actual geographical distribution of Sr and Nd isotopic compositions of the LTVF rocks (plot not shown) does not justify this interpretation, and seems to be consistent with the "sub-horizontal" slab inferred beneath the LTVF area (Lomnitz 1982). In any case, there should be evidence in trace element compositions supporting the addition of subduction fluids or melts, which is clearly not observed (see Fig. 7a–f and discussion below). Therefore, the isotopic diversity of the LTVF magmas is not likely to result from involvement of subducted slab. In fact, the LTVF rocks seem to show more a vertical spread (than a horizontal one) on the Sr–Nd isotope diagram (Fig. 5), which might be due to tapping of different regions of an isotopically heterogeneous mantle thorough the time span (~7 Ma to present) covered by these samples. Another observation worth commenting on is that several rocks from arcs including the CAVA also do plot on the mantle array close to the LTVF rocks, suggesting a common mantle source for both the CAVA and the LTVF.

Finally, the involvement of the "Downgoing slab" in the genesis of the LTVF magmas is also not favoured by other isotope systematics because the $^{87}Sr/^{86}Sr$, $^{206}Pb/^{204}Pb$, and $^{208}Pb/^{204}Pb$ data (Fig. 6a, d) require only a small sediment component (~1–5%), whereas the $^{143}Nd/^{144}Nd$ and $^{206}Pb/^{204}Pb$ data (Fig. 6b) are only compatible with a much higher sediment component (~5–30%, inconsistent with the other isotopes) and the $^{207}Pb/^{204}Pb$ data (Fig. 6c) cannot be easily reconciled by this process. On the other hand, the unpublished data by Sadofsky and Hoernle from the subducting Cocos plate (see individual data plotted in Fig. 6) also cannot explain the isotopic characteristics of the LTVF magmas

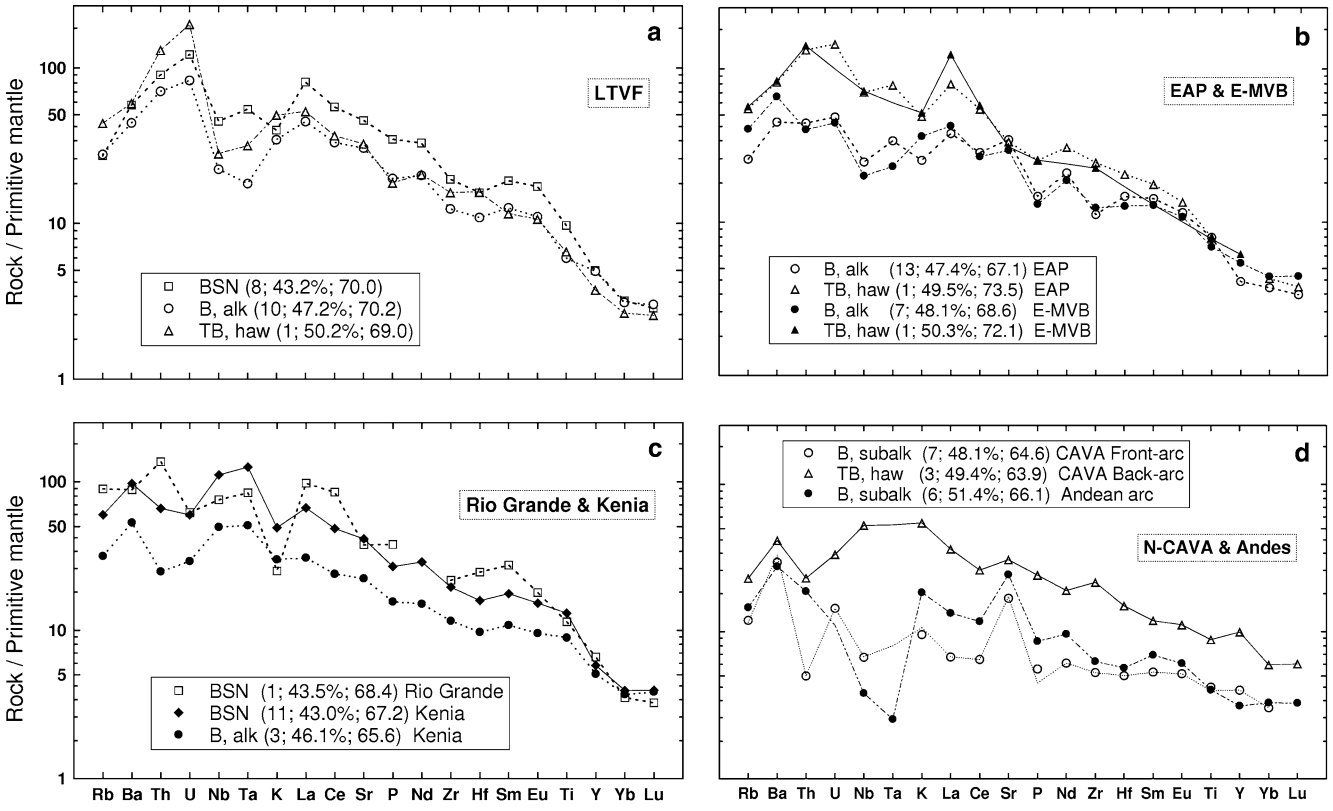

Fig. 4 Primitive mantle-normalized multi-element diagrams for representative primitive rocks from **a** LTVF; **b** EAP and E-MVB; **c** rifts represented by Rio Grande and Kenia; and **d** northern CAVA and the Andean continental arc. The samples are identified by their rock types as well as $(SiO_2)_{adj}$ and Mg# in *parentheses*. For rock types see the explanation of Fig. 2 (*alk* alkaline, *subalk* sub-alkaline). The primitive mantle values (μg/g) for normalization are from Sun and McDonough (1989): Rb 0.635; Ba 6.989; Th 0.085; U 0.021; Nb 0.713; Ta 0.041; K 250; La 0.687; Ce 1.775; Sr 21.1; P 95; Nd 1.354; Zr 11.2; Hf 0.309; Sm 0.444; Eu 0.168; Ti 1,300; Y 4.55; Yb 0.493; Lu 0.074

because most of the LTVF samples would fall away from any possible basalt–sediment mixing curve.

Trace elements and their ratios as subduction or mantle signals

In all bivariate diagrams (Fig. 7a–f) constructed using only primitive rocks, the chemical characteristics of the LTVF rocks summarized above and the fact that the LTVF rocks occupy a field distinct from most arc rocks but similar to rift rocks are also indicative of a negligible slab contribution in the LTVF rocks. As an example, both $[La/Yb]_{ChN}$ and $[La/Sm]_{ChN}$ values (chondrite-normalized ratios) for the LTVF rocks are similar to those of magmas from rifts and extension-related areas, and distinct from (higher than) the arcs, including the CAVA, and even the continental break-up areas (Fig. 7e).

Similarly, a negative Nb anomaly (here quantified by the parameter $[Nb/Nb^*_1]_{Primitive\text{-}mantle}$ or $[Nb/Nb^*_2]_{Primitive\text{-}mantle}$) commonly believed to be a diagnostic feature of an arc environment is also a common feature of primitive rocks from rifts, extension-related regions, and continental break-up areas (Fig. 7c, d). The main difference is that in arcs the negative Nb anomaly is accompanied by low Nb concentrations, whereas in rifts (and the LTVF) it is associated with relatively higher Nb contents. One may argue that because the concentration of a highly incompatible element such as Nb or Zr depends not only on the source concentration but also on the degree of melting, this distinction is not important. In fact, the distinction between arcs and rifts persists even when new combined bivariate diagrams between $[Nb/Nb^*_1]_{Primitive\text{-}mantle}$ or $[Nb/Nb^*_2]_{Primitive\text{-}mantle}$ parameter against Ba/Nb, Sr/P, Rb/La, Cs/Th, Ba/La, K/La, or Zr/Nb (some of these ratios are slab-indicative; Fig. 7) are prepared (plots not shown) where these ratio parameters are relatively less sensitive to the degree of mantle melting (than Nb concentration).

Another important point to note in most of the plots in Fig. 7 is that magmas from continental break-up areas (initiation of rifting) have lower concentrations of HFSE as compared to mature rifts. Finally, I propose that low values of the combined normalized parameters $[LILE_E/LREE_E]$ and $[LILE_E/HFSE_E]$ are excellent indicators of a rift environment as is the case of the LTVF (Fig. 7f), whereas their high values are diagnostic of an arc setting.

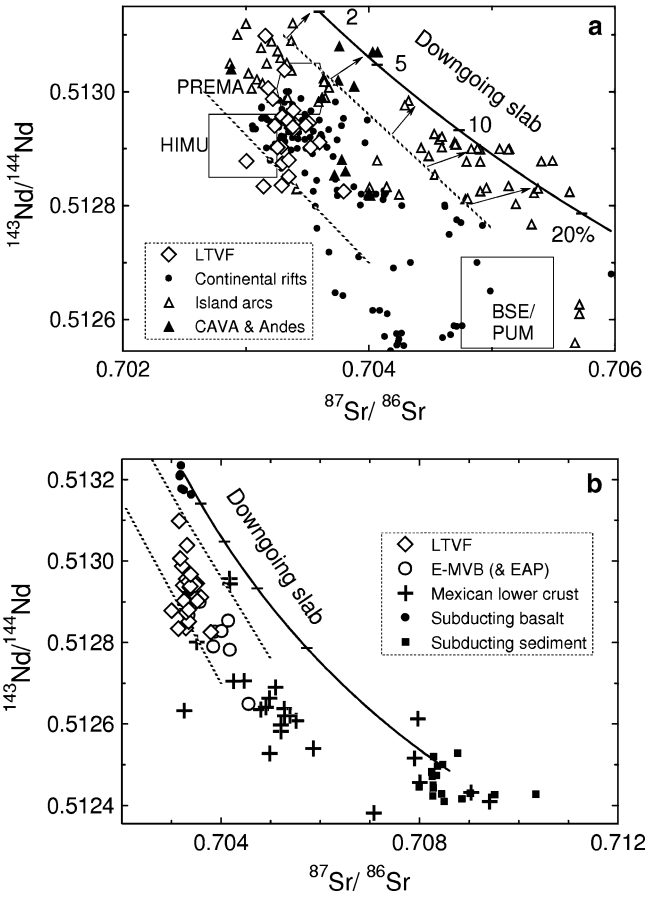

Fig. 5 $^{87}Sr/^{86}Sr$–$^{143}Nd/^{144}Nd$ plot for the LTVF primitive rocks and their comparison with other tectonic areas, mantle and crustal reservoirs, and the downgoing slab. The *symbols* used are shown as *inset* in each figure. Trace of the "mantle-array" (*dashed lines*) is included for reference (Faure 1986). **a** The LTVF rocks are compared with similar primitive rocks [Mg# > 63; $(SiO_2)_{adj} < 52\%$] from continental rifts including extension-related areas as well as from island and continental arcs including the northern part of the CAVA; all mantle components named after Zindler and Hart (1986) are: *BSE* bulk silicate earth or *PUM* primitive uniform mantle reservoir; *PREMA* prevalent mantle composition; *HIMU* high U/Pb mantle component. Also included is the mixing line (*thick solid curve*) of two-component mixing of altered basalts and sediments from the downgoing Cocos plate (Verma 2002); this is designated as "Downgoing slab". The *numbers* (2–20%) indicate the %m/m of the sediment component in this mixture. Note the shift towards the "Downgoing slab" shown by numerous arc magmas (schematically represented by *arrows*). **b** The LTVF rocks are compared with similar primitive rocks from the E-MVB (and the overlap region of the EAP with the MVB; Fig. 1), Mexican lower crust, and altered basalt and sediments from the subducting Cocos plate ("Downgoing slab"); the basalt–sediment mixing curve is the same as in **a**

Hofmann et al. (1986) showed that Ocean Island basalts (OIB) have Nb/U ratios of ~47 ± 10. The LTVF primitive rocks have considerably lower Nb/U values (4–18) that are similar to continental crust, whereas most rift rocks plot around this mean OIB value although some primitive rocks from rifts and continental break-up areas do have even lower Nb/U ratio than the LTVF rocks (Fig. 8a). Numerous arc rocks also have low values of Nb/U ratio but also show significantly lower Nb concentrations than the LTVF rocks. These low Nb/U values for the LTVF magmas are puzzling and show a strongly fractionated nature of the mantle source, which might have undergone one or more metasomatic events. However, these metasomatic fluids should not have originated from downgoing slab because in the LTVF primitive rocks the fluid-diagnostic ratios such as Ba/Nb, Sr/P, etc. (Fig. 7a–f) are not "arc-like". Furthermore, although the subduction fluids might mobilize U (due to its higher solubility in an oxidized state), Th mobilization, and, consequently, high Th/U, Th/Ba, and Th/Rb ratios for the LTVF rocks (Fig. 4a), are difficult to explain by such a process.

Nevertheless, to understand if the rocks were derived from an HFSE-depleted source similar to that of arc rocks, I followed the methodology by Pearce and Parkinson (1993) and Pearce and Peate (1995) to study subduction zone processes. Geochemical data for primitive rocks were plotted in two additional bivariate diagrams (Fig. 8b, c) using elements (two HFSE Nb and Ti; one heavy REE Yb; plots for other HFSE are not shown) that are not added during the subduction process. Both plots clearly show that the LTVF rocks are not depleted in HFSE at a given Yb concentration level as compared to most arc rocks as well as continental break-up rocks. Pearce and Parkinson (1993) used a Ti versus Yb diagram to distinguish between garnet lherzolite and spinel lherzolite sources. As a conclusion, it appears that, as compared to arc sources, the source of the LTVF magmas is enriched in all HFS elements (Nb, Ti, etc.) but more so in U and Th (both of them are also characterized by high ratio of ionic charge to ionic radius, i.e. both are also HFS elements according to Weaver 1991 and Rollinson 1993). The reason for this greater enrichment of U and Th over Nb and other HFSE is not clear at present. However, very diverse mantle fluids such as those enriched in LREE, Th, U, over other elements like Nb, Ta, etc. are known to exist in extension-related areas (Ionov et al. 1994). Finally, if this enrichment were from subduction fluids, then why other ratios, such as Ba/Nb, Sr/P, Rb/La, Cs/Th, $[Nb/Nb^*_1]_{Primitive\text{-}mantle}$, $[Nb/Nb^*_2]_{Primitive\text{-}mantle}$, Ba/La, Zr/Nb, La/Yb, La/Sm, $[LILE_E/LREE_E]$, and $[LILE_E/HFSE_E]$ or Nb and Zr concentrations (Fig. 7a–f; other plots not shown), do not show clear effects of such fluids?

To learn further about the significance of the negative Nb anomaly in the LTVF rocks, I have calculated statistical parameters for $[Nb/Nb^*_2]_{Primitive\text{-}mantle}$ (Table 3) from the worldwide databases established in the present work. All arcs around the world show, without exception, very large negative Nb anomalies (median and mean values ~0.06–0.32; 95 and 99% confidence limits within the range of ~0.03–0.47 and ~0.01–0.60, respectively). The LTVF rocks show significantly smaller negative Nb anomalies as compared to all arcs (mean or median value of ~0.60; 95 and 99% confidence limits of 0.53–0.71 and 0.50–0.74, respectively). Furthermore,

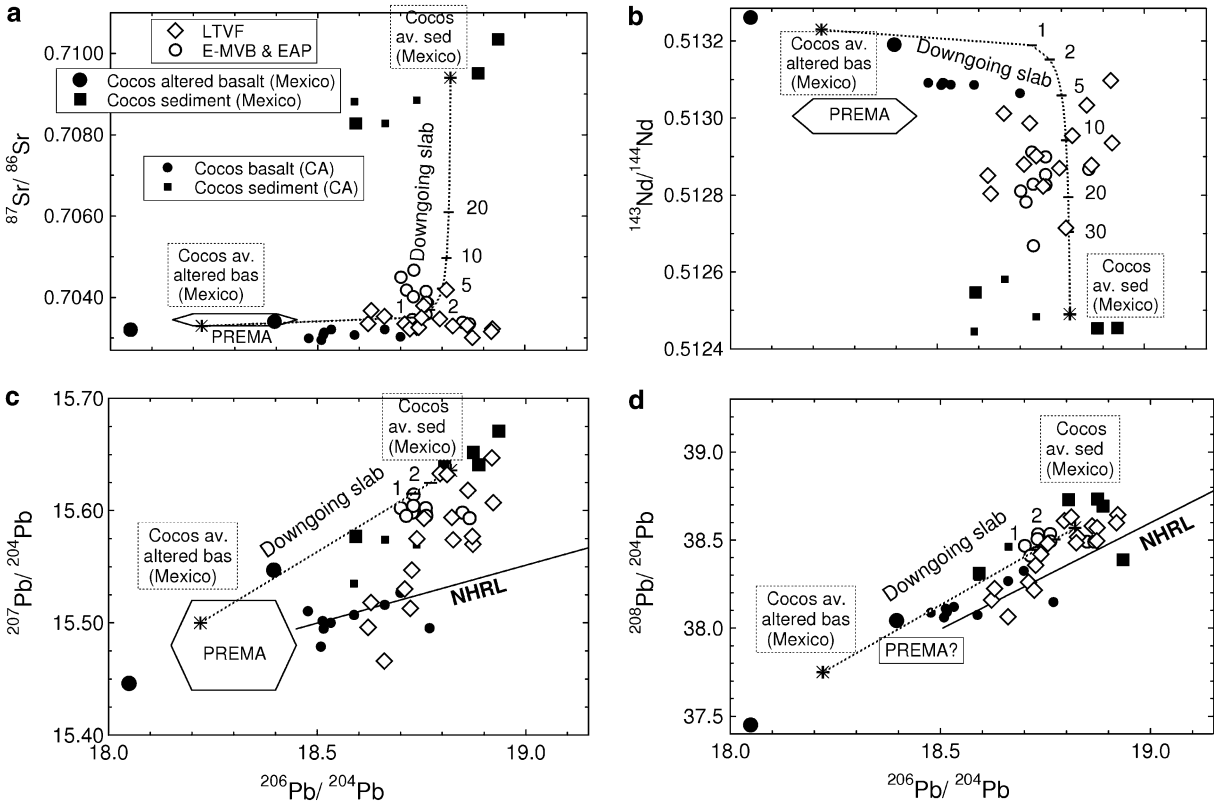

Fig. 6 Isotope–isotope diagrams for the LTVF primitive rocks and comparison with similar rocks from the E-MVB (and the overlap region of the EAP with the MVB; Fig. 1). The *symbols* used are given as *inset* in **a**. The data for altered basalt and sediment samples from the Cocos plate as well as their mixing curve (designated "Downgoing slab") is also shown (the *numbers* 1, 2, 5, 10, 20, and 30 refer to the %m/m of the sediment component in this basalt–sediment mixture). The basalt and sediment data for the downgoing slab are from Verma (2000b) for the Mexican part (IPOD-DSDP Leg 68, Sites 487 and 488) and from S.J. Sadofsky and K. Hoernle (in preparation) for the Central America part (ODP Leg 206, Site 1256; 91.934°W, 6.736°N; note this location is outside the map of Fig. 1) of the Cocos plate. The Northern Hemisphere Reference Line (NHRL; Hart 1984) is included as a reference in Pb–Pb plots. The mantle component PREMA (Zindler and Hart 1986) is also shown; the other components plot somewhat outside of the field of these figures. Note rocks from the Mexican lower crust could not be plotted here because unfortunately Pb isotope data are still not available for them. **a** $^{206}Pb/^{204}Pb$–$^{87}Sr/^{86}Sr$; **b** $^{206}Pb/^{204}Pb$–$^{143}Nd/^{144}Nd$; **c** $^{206}Pb/^{204}Pb$–$^{207}Pb/^{204}Pb$; and **d** $^{206}Pb/^{204}Pb$–$^{208}Pb/^{204}Pb$

the size of the LTVF Nb anomaly is statistically identical to those of the negative anomalies observed in numerous rifts, extension-related areas, and continental break-up regions as well as two other Mexican provinces (see the areas classified under the subtitle of "with negative Nb anomaly" in Table 3). This is an important observation contrary to the general belief that basic and ultrabasic rocks from rifts and extension-related and continental break-up regions possess only positive or no Nb anomalies; in fact, more regions show an overall negative rather than a positive Nb anomaly. I, therefore, conclude that the cause of the negative Nb anomaly in the LTVF is similar to that for rifts (i.e. similar mantle sources and related processes of the addition of metasomatic fluids and pressure-released melting) but totally distinct from the (subduction) processes of arc formation.

In summary, I suggest that rifts, extension-related areas, and continental break-up regions such as Central Afar, East China, or Kwanza, with a positive Nb anomaly (Table 3), are likely to have a significant contribution from the asthenosphere—the deeper part of the mantle underlying the lithosphere that has been probably modified by incorporating residual subducted slabs. On the other hand, the source of extensional regions such as Basin and Range, North and Northeast China, and the LTVF with a negative Nb anomaly (Table 3) should dominantly reside in the lithosphere. Thus, the presence of a negative Nb anomaly in numerous rifts may be related to the nature of the lithospheric sources and the deeper metasomatic fluids, if any, that might have facilitated mantle melting under extensional conditions.

Discrimination diagrams indicative of a rift setting

Major and trace element based discrimination diagrams have been widely used to infer tectonic setting (e.g. Rollinson 1993). As additional constraints, several conventional and new discrimination diagrams were constructed for LTVF basic rocks (all primitive as well as evolved rocks with $SiO_2 < 52\%$). In all of these

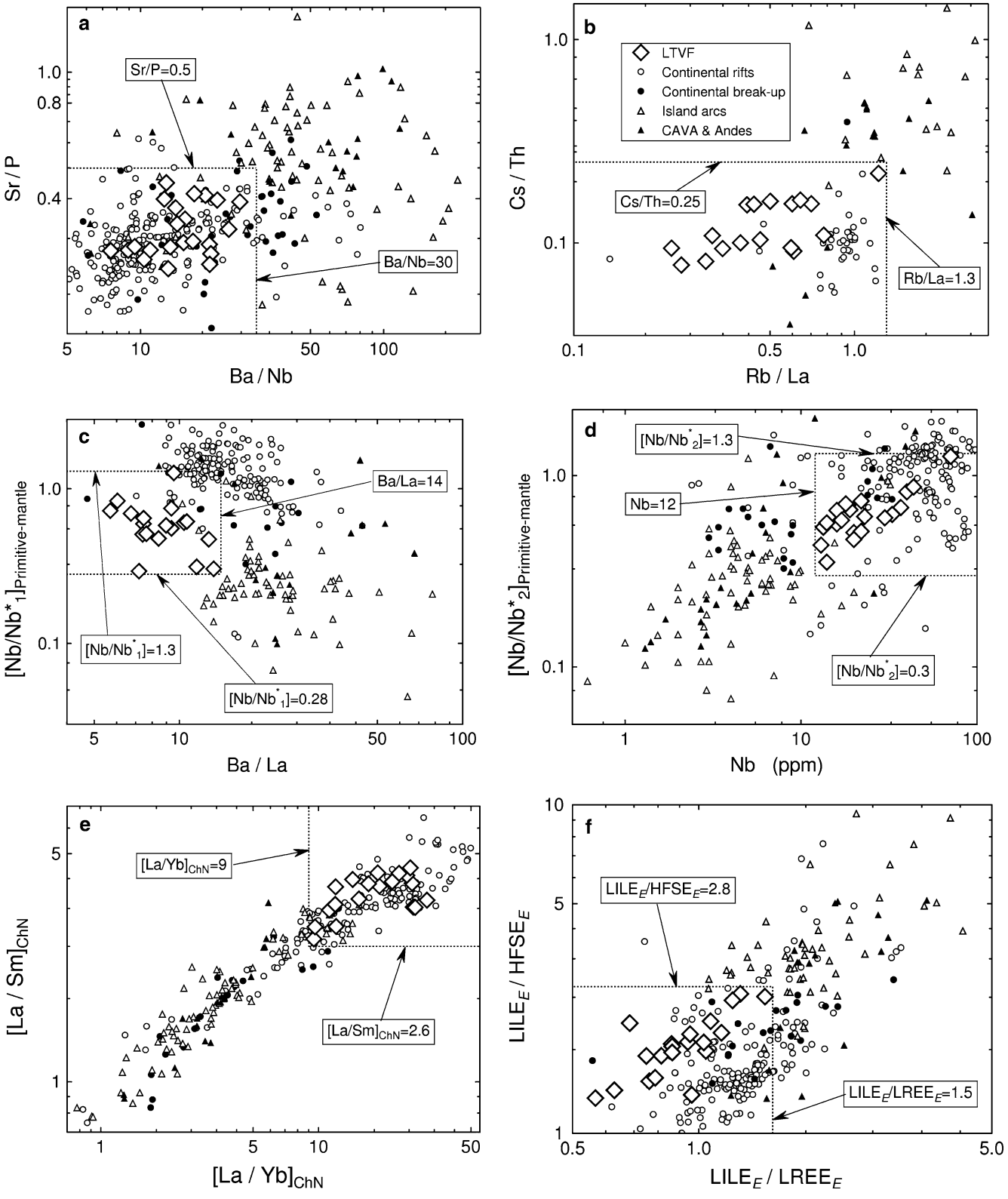

diagrams (some are shown in Figs. 9, 10, 11, 12), the compiled data from arcs and rifts were also plotted to check their general functioning, but to keep the diagrams simple these data are shown only in Fig. 11 (with Fig. 12 also showing the CAVA rocks).

In Ti/Y–Zr/Y diagram (Fig. 9a) most LTVF rocks (21 out of 26 samples; ~81%) plot in the "Within-plate" field. In Zr–Zr/Y diagram (Fig. 9b) almost all samples plot in the "Within-plate" field (with the exception of two samples that plot in the MORB field; it is

◄

Fig. 7 Six binary diagrams constructed using slab-sensitive or mantle-sensitive parameters, for primitive rocks from the LTVF and their comparison with similar rocks from continental rifts including extension-related areas and continental break-up regions as well as from island and continental arcs including the northern part of the CAVA. The *symbols* used are shown as *inset* in **b**. *Dotted lines* in different diagrams give approximate reference values for the fields occupied by the LTVF primitive rocks. **a** Slab-sensitive Ba/Nb-slab-sensitive Sr/P (therefore, both parameters are likely to have high values for arcs); **b** slab-sensitive Rb/La-slab-sensitive Cs/Th; **c** slab-sensitive Ba/La–$[Nb/Nb^*_1]_{Primitive\text{-}mantle}$, where $[Nb/Nb^*_1]_{Primitive\text{-}mantle}$ is a quantitative measure of Nb anomaly defined as the ratio of actually measured Nb concentration of a sample normalized with respect to (w.r.t.) primitive mantle and the average value of primitive mantle-normalized concentrations of Th and K in the same sample (Nb^*_1 is thus the primitive mantle-normalized Nb value "*required for a smooth multi-element pattern*" w.r.t. the neighbouring elements Th and K in multi-element diagrams such as Fig. 4 (primitive mantle values were from Sun and McDonough 1989); **d** mantle-sensitive Nb–$[Nb/Nb^*_2]_{Primitive\text{-}mantle}$, where $[Nb/Nb^*_2]_{Primitive\text{-}mantle}$ is a quantitative measure of Nb anomaly defined as the ratio of actually measured Nb concentration of a sample normalized w.r.t. primitive mantle and the average value of primitive mantle-normalized concentrations of Ba and La in the same sample (primitive mantle values were from Sun and McDonough 1989); **e** mantle-sensitive $(La/Yb)_{ChN}$-mantle-sensitive $(La/Sm)_{ChN}$ where the subscript $_{ChN}$ refers to chondrite-normalized values (the same as in Fig. 3); and (f) slab-sensitive $[LILE_E/(LREE_E]$-slab-sensitive $[LILE_E/HFSE_E]$ (both ratios are excellent parameters recently used by Verma 2004) where subscript E refers to silicate earth-normalized values, $LILE_E = (K_E + Rb_E + Ba_E + Sr_E)/4$, $LREE_E = (La_E + Ce_E + Nd_E)/3$, $HFSE_E = (Nb_E + Zr_E + Ti_E + P_E)/4$. All concentration data in μg/g were normalized against silicate earth values (E) given by McDonough and Sun (1995): K 240, Rb 0.600, Ba 6.600, Sr 19.9, La 0.648, Ce 1.675, Nd 1.250, Nb 0.658, Zr 10.5, Ti 1,205, P 90

noteworthy that not even one sample plots in the field of arcs). In Ti–V diagram (Fig. 9c) the LTVF samples plot in the field of MORB and OIB and not in the field of arcs. In principal component Score 1–Score 2 diagram, based on Ti, Zr, Y, and Sr concentrations and log transformations (Fig. 9d), all but four samples plot in the "Within-plate" field. A relatively new set of bivariate discrimination diagrams based on Nb and Ba (Vasconcelos et al. 1998) was also constructed (plots not shown), according to which the LTVF magmas plot in the combined field of "Rift and Ocean Island" and not in the "Continental and Island arcs" field.

In two ternary diagrams (Figs. 10 and 11) most LTVF rocks plot in the field of "Within-plate" and "Continental" basalts, respectively, and not in the arc field. Rift and arc data from our database, also plotted in Fig. 11, show a general functioning of this diagram (on a statistical basis) for discrimination purposes. However, the diagram does not seem to work well for the CAVA rocks, which plot in all three areas, although most of them do so in the arc basalt field.

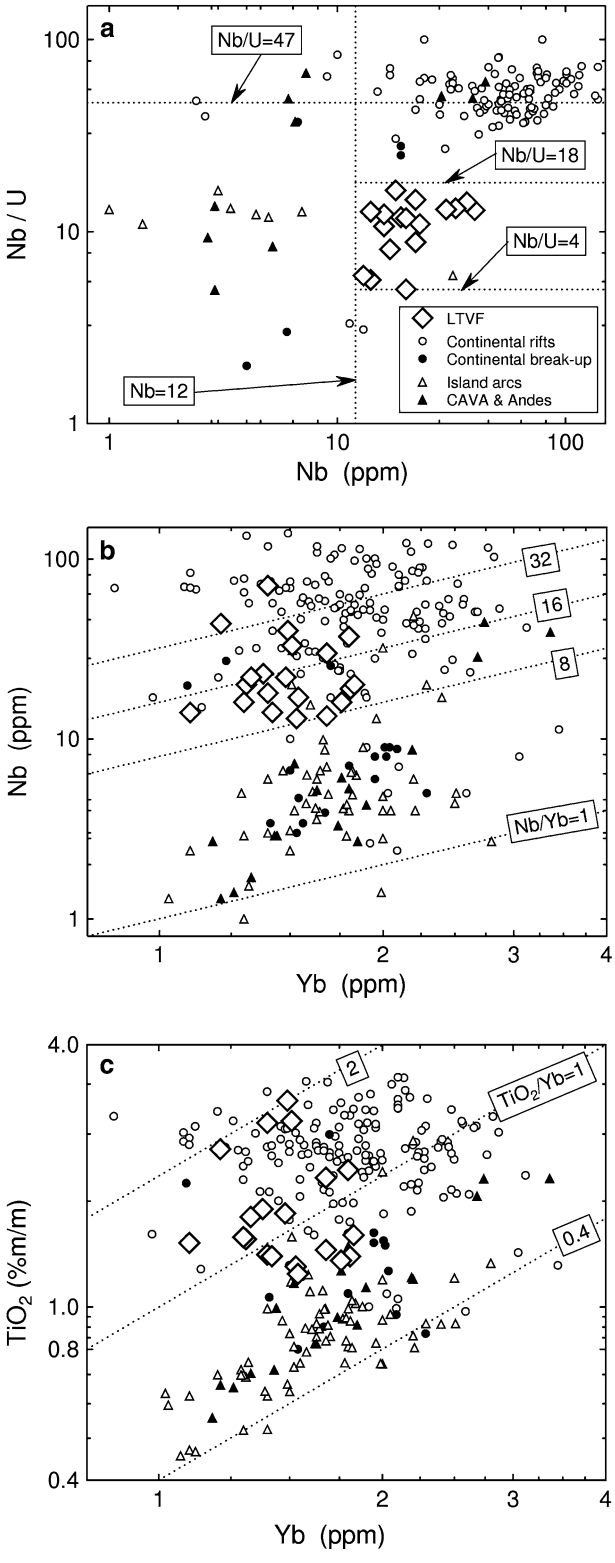

►

Fig. 8 Three binary diagrams for primitive rocks from the LTVF and their comparison with similar rocks from continental rifts, including extension-related and continental break-up areas, as well as from island and continental arcs, including the northern part of the CAVA. The *symbols* used are shown as *inset* in **a**. *Dotted lines* in different diagrams give approximate reference values. **a** Nb–Nb/U (Nb/U reference value of 47 is the average value for OIB from Hofmann et al. 1986); **b** Yb–Nb; and **c** Yb–$(TiO_2)_{adj}$ (the subscript adj refers to the adjusted value from the SINCLAS program by Verma et al. 2002). The latter two diagrams are useful to show mantle source characteristics because the respective elements are not significantly added during subduction processes

Table 3 Statistical data for the Nb anomaly (w.r.t. Ba and La) for basic and ultrabasic rocks from the LTVF (Mexico) and their comparison with arcs, rifts, extension-related areas, and continental break-up regions around the world as well as with other Mexican provinces

Area	n	$\tilde{x}$	$\bar{x} \pm s$	95% CL	99% CL
LTVF (Mexico)	22	0.61	0.62 ± 0.20	0.53–0.71	0.50–0.74
Arcs					
Aleutian arc	13	0.11	0.19 ± 0.08	0.14–0.24	0.12–0.26
	11[a]	0.15	0.17 ± 0.06	0.13–0.21	0.11–0.22
Burma arc	4	0.09	0.09 ± 0.02	0.05–0.13	0.02–0.16
Central American Volcanic Arc (CAVA)	55	0.13	0.17 ± 0.13	0.14–0.21	0.13–0.22
Izu-Bonin arc	18	0.09	0.16 ± 0.21	0.06–0.27	0.02–0.31
	16[a]	0.09	0.10 ± 0.05	0.07–0.13	0.06–0.14
Japan arc	7	0.14	0.19 ± 0.15	0.05–0.33	–
	6[a]	0.14	0.15 ± 0.09	0.05–0.24	–
Kamchatka arc	14	0.21	0.34 ± 0.35	0.14–0.54	0.07–0.62
	12[a]	0.21	0.22 ± 0.11	0.15–0.29	0.12–0.32
Lesser Antilles arc	45	0.31	0.32 ± 0.12	0.28–0.35	0.28–0.36
Luzon arc	4	0.31	0.30 ± 0.10	0.14–0.47	~0.01– 0.60
Marianas arc	8	0.07	0.07 ± 0.04	0.04–0.11	0.02–0.12
New Hebrides arc	10	0.14	0.16 ± 0.04	0.12–0.19	0.11–0.20
Papua-New Guinea arc	3	0.11	0.09 ± 0.02	0.04–0.15	–
Philippines arc	20	0.22	0.21 ± 0.07	0.18–0.25	0.17–0.26
Sangihe arc	3	0.16	0.16 ± 0.01	0.13–0.19	0.09–0.23
Sunda-Banda arc	23	0.15	0.15 ± 0.08	0.11–0.18	0.10–0.20
Tonga-Kermadec arc	8	0.14	0.15 ± 0.08	0.08–0.22	0.05–0.26
Vanuatu arc	5	0.06	0.06 ± 0.02	0.03–0.09	0.01–0.11
Rifts and extension-related areas: with negative Nb anomaly					
Basin and Range (BR, USA)	34	0.64	0.69 ± 0.33	0.58–0.81	0.54–0.85
Colorado Plateau-Transition. BR (USA)	39	0.63	0.63 ± 0.19	0.57–0.69	0.50–0.74
Rio Grande rift	35	0.81	0.77 ± 0.43	0.62–0.91	0.57–0.97
Western USA	30	0.68	0.73 ± 0.39	0.58–0.88	0.53–0.93
North China	8	0.85	0.84 ± 0.08	0.77–0.90	0.74–0.93
Northeast China	22	0.79	0.78 ± 0.22	0.69–0.88	0.65–0.91
Gregory rift (Kenya)	4	0.74	0.77 ± 0.08	0.64–0.90	0.53–1.01
Rifts and extension-related areas: with practically no Nb anomaly					
Abu Gabra rift (Sudan)	8	0.98	0.98 ± 0.19	0.82–1.14	0.74–1.22
Ethiopian rift	47	1.03	0.97 ± 0.19	0.91–1.03	0.90–1.15
East African rift	47	1.09	1.05 ± 0.29	0.97–1.14	0.92–1.19
Rifts and extension-related areas: with positive Nb anomaly					
Central Afar (Ethiopia)	13	1.16	1.20 ± 0.28	1.03–1.37	0.96–1.43
East China	86	1.24	1.21 ± 0.25	1.15–1.26	1.14–1.28
Southeast China	25	1.58	1.57 ± 0.30	1.45–1.69	1.40–1.74
Massif Central (France)	21	1.51	1.52 ± 0.19	1.44–1.61	1.41–1.64
Continental break-up regions: with negative Nb anomaly					
Columbia River	3	0.37	0.41 ± 0.12	0.12–0.70	–
Deccan (India)	12	0.59	0.61 ± 0.19	0.49–0.73	0.44–0.78
Greenland	3	0.79	0.82 ± 0.09	0.59–1.05	0.29–1.36
Paraná	1	–	0.49	–	–
Continental break-up regions: with positive Nb anomaly					
Kwanza	2	–	1.41 ± 0.05	0.9–1.9	–
Wrangellia	1	–	1.41	–	–
Other Mexican Provinces					
Eastern Alkaline Province	97	0.76	0.80 ± 0.27	0.74–0.85	0.72–0.86
Eastern Mexican Volcanic Belt	94	0.49	0.53 ± 0.22	0.48–0.57	0.46–0.59

For CAVA, some basalts from the back-arc Yohoa volcano (Fig. 1) showing significant positive Nb anomaly were not included in the statistical calculations, otherwise the statistics were not meaningful

n number of samples; $\tilde{x}$ median; $\bar{x}$ mean; s standard deviation; 95% *CL* 95% confidence limit of the mean; 99% *CL* 99% confidence limit of the mean. – means that the 99% confidence limits were not meaningful for these more dispersed parameters because of the very small number of samples

[a]When the median ($\tilde{x}$) and mean ($\bar{x}$) values for the Nb anomaly showed significant differences, the data were checked for outliers (Verma et al. 1998); for these cases, the statistical data are also presented after outlier detection and elimination

Nevertheless, the LTVF rocks occupy a different area, away from Y/15-apex, as compared to the CAVA rocks; most of the latter plot closer to this apex. Basic and differentiated rocks from the LTVF plot mostly in the Ocean Island field in the $10MnO–TiO_2–10P_2O_5$ ternary diagram (after Mullen 1983; plot not shown). However, in another ternary diagram (Th-Hf/3-Ta after Wood 1980; plot not shown) most LTVF rocks plot in the field of volcanic arc basalts because of their very high Th contents.

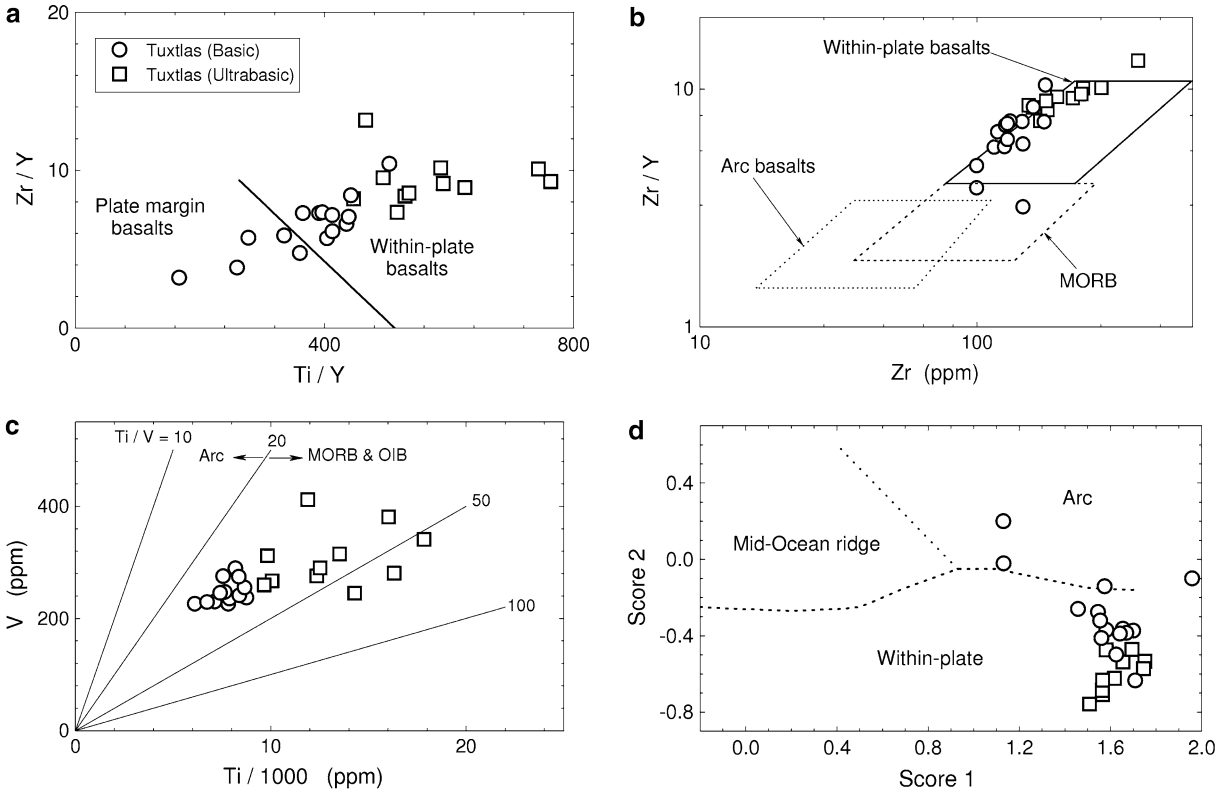

Fig. 9 Binary discrimination diagrams for the LTVF basic and ultrabasic rocks. Note all diagrams indicate a "Within-plate" ("Continental rift") setting for the LTVF. **a** Ti/Y–Zr/Y (after Pearce and Gale 1977); **b** Zr–Zr/Y (after Pearce and Norry 1979); **c** Ti–V (after Shervais 1982); and **d** Score 1–Score 2 (after Butler and Woronow 1986)

A set of five new discriminant function diagrams has recently been proposed (Agrawal et al. 2004). These diagrams are based on the statistical method of linear discriminant analysis of major elements in an extensive compilation of Pliocene to Recent basic rocks from four tectonic settings. These statistics-based diagrams showed the rate of correct classification ranging from

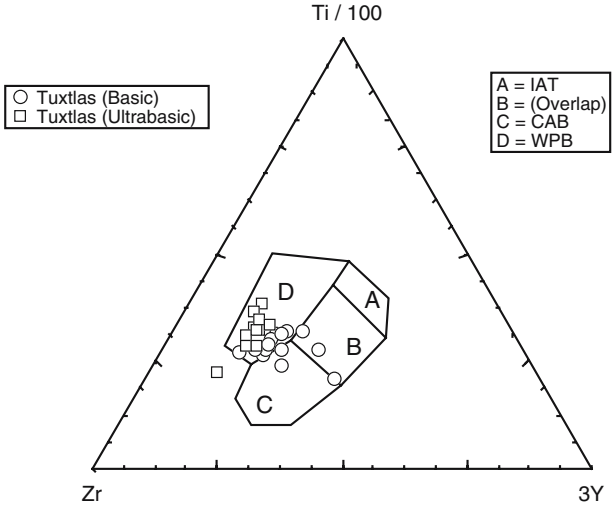

Fig. 10 Zr-Ti/100-3Y ternary discrimination diagram for the LTVF basic and ultrabasic rocks (after Pearce and Cann 1973). Note this diagram indicates a "Within-plate" ("Continental rift") setting for the LTVF. *IAT* island arc tholeiite, *B* overlap region, *C* calc-alkaline basalt, *D* within-plate basalt

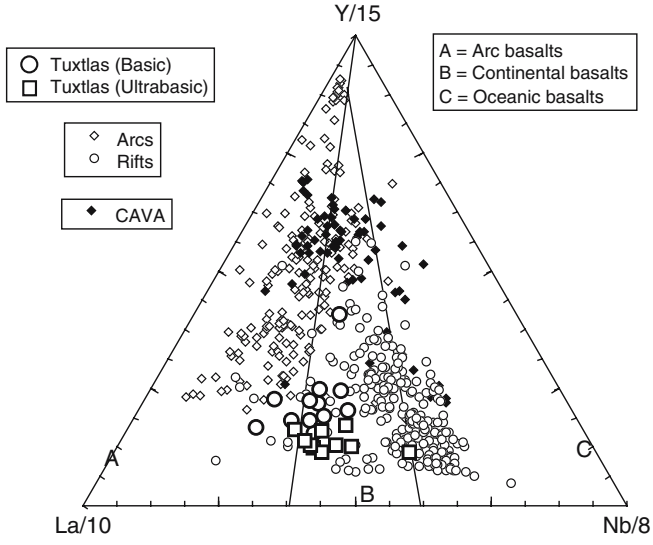

Fig. 11 La/10-Y/15-Nb/8 ternary discrimination diagram for the LTVF basic and ultrabasic rocks (after Cabanis and Lecolle 1989). Note this diagram indicates a "Within-plate" ("Continental rift") setting for the LTVF. Data for arcs, including the CAVA, and rifts from this compilation are also shown to check the statistical functioning of this diagram for discriminating arc and rift rocks

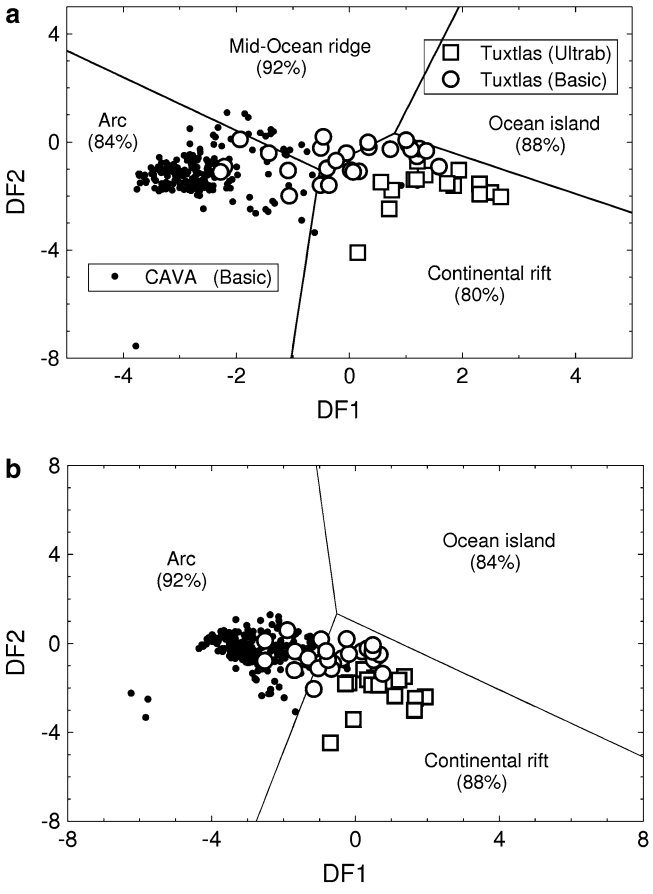

Fig. 12 Two discriminant function diagrams for the LTVF basic and ultrabasic rocks (after Agrawal et al. 2004). The per cent given next to the tectonic setting name represents the per cent success obtained by these authors during the testing stage of these diagrams. The *symbols* used are shown as *inset* in **a**. Note both diagrams indicate a continental rift setting for the LTVF magmas, and an arc setting for the CAVA. **a** Four tectonic settings (Arc-Continental rift-Ocean Island-Mid-Ocean ridge); and **b** three tectonic settings (Arc–Continental rift–Ocean Island)

76 to 96%. The use of these discriminant function diagrams is recommended on such a statistical basis. In other words, if a high percentage of basic rocks from a given area consistently plot in a given tectonic setting in four of these diagrams (the fifth diagram will not have the predicted field), the tectonic setting can be inferred with confidence for that particular area. Two such diagrams for the LTVF rocks (Fig. 12; other diagrams proposed by Agrawal et al. 2004, provided similar results and, therefore, are not presented here) clearly show a "Continental rift" setting for them (~76% of the LTVF rocks plot in this field in Fig. 12a, whereas ~82% do so in Fig. 12b). Note that the CAVA rocks mostly plot in the "arc" field, confirming, thus, the functioning of these diagrams for inferring tectonic settings.

I, therefore, conclude that the tectonic setting inferred from the use of the discrimination diagrams (Figs. 9, 10, 11, 12) is a "Continental rift" and not an arc.

Table 4 Statistical data for linear correlations between two variables for primitive rocks from the LTVF and some representative arcs

Area	n	r	Slope ± 1 s	$[1-P_{c(r,n)}]$
Variables: $[Sr/Sr^*]_{MORB}$– Sr/Y				
LTVF	20	0.124	-0.004 ± 0.007	0.3988
Aleutian arc	8	0.892	0.137 ± 0.028	0.9971
CAVA	10	0.730	0.108 ± 0.036	0.9834
CAVA + Andes	15	0.504	0.045 ± 0.021	0.9444
Variables: Sr/P–Ba/Nb				
LTVF	20	0.305	0.0041 ± 0.0029	0.8326
Andes	11	0.876	0.0091 ± 0.0017	0.9996
Andes + CAVA	22	0.551	0.0036 ± 0.0012	0.9922

n number of data pairs available for the linear regression; r correlation coefficient of the linear model; s standard deviation; $[1-P_c(r,n)]$ the probability that the two variables are correlated; $[Sr/Sr^*]_{MORB}$ is a quantitative measure of Sr anomaly defined as the ratio of actually measured Sr concentration of a sample normalized with respect to an average MORB (Sun and McDonough 1989) and the average value of MORB-normalized concentrations of Ce and Nd in the same sample (Sr* is thus the MORB-normalized Sr value "*required for a smooth multi-element pattern*" with respect to the neighbouring elements Ce and Nd)

Further considerations against subduction-related melting

The subducting Cocos plate corresponding to the LTVF is relatively young (about 15–20 Ma; Burbach et al. 1984; Klitgord and Mammerickx 1988) and therefore, in principle, the slab could melt and generate magmas (e.g. Kay 1978; Defant et al. 1991b; Kay et al. 1993; Peacock et al. 1994; Proteau et al. 1999). Such a slab melt process is likely to give rise to high-Mg andesite or the so-called adakite rocks (e.g. Defant and Drummond 1990; Kay et al. 1993; Yogodzinski et al. 1995), or andesitic and dacitic rocks with high Sr/Y, low Y, and steep REE patterns (e.g. Morris 1995). Such magmas are not observed in the LTVF.

It is also possible that these slab melts may mix with the overlying mantle (loosing their identity as "adakites") and produce basic or even ultrabasic magmas. The slab melts are likely to have radiogenic isotopic compositions similar to the "Downgoing slab" as shown in Figs. 5 and 6 for the Cocos plate. The "Downgoing slab" curve represents a two-component basalt–sediment mixture of the slab. The isotopic compositions of the LTVF magmas should be shifted from "mantle values" towards downgoing slab (Figs. 5, 6), and this shift should be accompanied by a significant $[Sr/Sr^*]_{MORB}$ anomaly (Pearce 1982), which is not observed (plot not shown). Further, if the involvement of these slab melts in the LTVF magmas were true, we should observe a significant positive correlation between the size of the positive Sr anomaly ($[Sr/Sr^*]_{MORB}$) and the Sr/Y ratio because both these parameters are increased in the slab melts. Statistical data summarized in Table 4 show that no significant correlation exists between these parameters for the LTVF primitive rocks

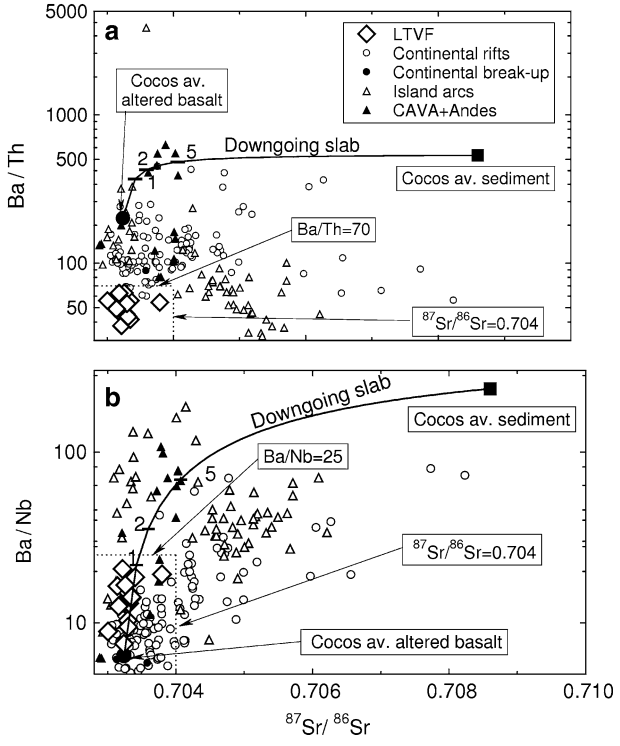

Fig. 13 Subducted slab-indicating ratios against $^{87}Sr/^{86}Sr$ for the LTVF primitive rocks and their comparison with similar rocks from continental rifts and break-up areas, island arcs, the northern CAVA, and the Andean continental arc. The *symbols* used are shown as *inset* in **a**. The reference lines that totally enclose the LTVF data are also shown. The average data for altered basalts and sediments from the subducting Cocos plate (Downgoing slab) as well as the simple binary mixing curve are also shown for reference; the *numbers* 1–5 refer to the sediment component (%) in the basalt–sediment mixture. **a** $^{87}Sr/^{86}Sr$–Ba/Th; and **b** $^{87}Sr/^{86}Sr$–Ba/Nb

($[1-P_c(r,n)]\sim0.40$, being $<<0.95$, i.e. not significant at 95% confidence level), whereas both Aleutian arc (an example of an island arc) and CAVA (continental arc) as well as the combined data from the CAVA and the Andes show such a systematic behaviour (statistically significant at ~95% confidence level). Similarly, other subduction-signal parameters (Sr/P–Ba/Nb) show a statistically significant positive correlation for primitive rocks from the Andes as well as the combined data for the Andes and CAVA, but not for the LTVF at 95% confidence level ($[1-P_c(r,n)]<0.95$; Table 4). Furthermore, slab melts from the Cocos plate would have pronounced Nb, Ti, and probably Eu and Ce negative anomalies, which should persist even after these slab melts mix with the mantle to produce magmas. None of these features is observed in the LTVF magmas.

Therefore, partial melting of the downgoing slab as the possible mechanism for the petrogenesis of the LTVF magmas, even indirectly, can be ruled out. Besides, even if such high-Mg intermediate magmas were present in the LTVF, this could not be taken as an exclusive characteristic of arcs. Such magmas have been observed also in other tectonic settings (such as rift and extension-related areas compiled in this work) and alternative mechanisms have been proposed to explain their occurrence (e.g. Fisk 1986).

It is known that fluids released from the downgoing slab can lower the melting point of mantle wedge materials, and thus produce magmas (Peacock 1990; McCulloch and Gamble 1991; Davies and Stevenson 1992; Nelson 1995; Pearce and Peate 1995; Harry and Green 1999). Subduction fluid-induced mantle melting would generate trace element characteristics that are typical of many arcs, including the CAVA. The LTVF magmas present characteristics that are significantly different from arcs but very similar to those of rifts and extension-related areas (see Figs. 7, 8, 9, 10, 11, 12).

Besides all these chemical features, high values of Ba/Th and Ba/Nb and positive relationships of these ratios with Sr isotopic ratios have been taken to infer the genesis of arc magmas by addition of subduction fluids to the mantle wedge (e.g. Hoogewerff et al. 1997; Turner et al. 1998; Kimura et al. 2001; Walker et al. 2001). Caution is, however, required because crustal contamination, particularly upper crustal contamination, can also cause a simultaneous increase in these element ratios as well as in Sr isotopic ratios. Only primitive rocks with a lesser probability of upper crustal contamination are plotted in Fig. 13. The LTVF rocks plot in narrow regions of low $^{87}Sr/^{86}Sr$, low Ba/Th (Fig. 13a) and low $^{87}Sr/^{86}Sr$, low Ba/Nb (Fig. 13b), similar to well-known continental rifts, and do not represent arc-type characteristics (high values of these parameters). Because of unusually high Th enrichment the LTVF rocks show still lower Ba/Th ratios than most rifts (Fig. 13a). Note no arc rocks plot in the field represented by LTVF in Fig. 13a, in which low values of Ba/Th in some arc rocks are accompanied by high $^{87}Sr/^{86}Sr$. Average values for these parameters in altered basalts and sediments as well as simple binary mixing curves for the downgoing slab are also plotted in Fig. 13. Although the LTVF rocks fall close to the slab mixing curve in Fig. 13b and the required sediment component is only ~1%, the combined $^{87}Sr/^{86}Sr$–Ba/Th data (Fig. 13a) cannot be reconciled by such a slab involvement process because the mixing curve lies far away from the LTVF data. Therefore, subduction fluid-induced models can also be ruled out for the LTVF mantle source.

Heterogeneous mantle melting: inverse modelling of trace element data and implications for the origin of primitive magmas

The failure of the slab-involvement models suggests that the LTVF magmas were generated solely in the underlying mantle. According to the criteria of Pearce and Peate (1995), the LTVF primitive rocks (with Nb/Yb~8–50; Ti (in %m/m)/Yb (μg/g)~0.4–1.2;

Th/Yb~2.3–8.4; Zr/Yb~70–200) would fall on the enriched side of the diagrams, even outside the field of their Fig. 2a–c (not reproduced here), implying that the LTVF source is more enriched than average N-MORB or even E-MORB compositions. The highly steep slopes of chondrite-normalized REE plots observed for primitive rocks from the LTVF (Fig. 3) and the consequently high $[La/Yb]_{ChN}$ values (Fig. 7e) would be consistent with residual garnet in this mantle source region (e.g. Kay and Gast 1973; Nelson et al. 1995; van Westrenen et al. 2001). Nelson et al. (1995) also noted that the presence of a small positive Eu anomaly in many primitive rocks and the absence of petrographic evidence of plagioclase accumulation. They concluded that this observation points to a source with residual clinopyroxene in spite of the fact that the behaviour of Eu is sensitive to oxygen fugacity in the mantle. Pressure-released melting of the mantle and subsequent melt extraction are possible in any tectonic environment, including arcs (e.g. McKenzie and Bickle 1988; Kostopoulos 1991; Kostopoulos and James 1992; Williamson et al. 1995; Sisson and Bronto 1998; Wang et al. 2002). The extensional regime mapped in the LTVF by Nelson and Gonzalez-Caver (1992) and Nelson et al. (1995) is consistent with such a model of pressure-released mantle melting.

Because of the somewhat heterogeneous nature of this mantle source (the isotopic compositions of the LTVF magmas are not really uniform but show a range of values), it would appear that inverse modelling of trace element data for primitive magmas might not be strictly valid. However, primitive magmas are abundant in the LTVF, such a modelling is, therefore, considered useful to understand the nature of "average" source characteristics (Minster and Allègre 1978; Albarède 1983; Hofmann and Feigenson 1983; Hofmann et al. 1984; McKenzie and O'Nions 1991; Ormerod et al. 1991; Maaløe 1994; Velasco-Tapia and Verma 2001; Verma 2004). The samples that were used for this purpose have low SiO_2 (42.3–50.2 adjusted %m/m), low FeO^T/MgO (0.67–1.03), high MgO (8.9–15.8%m/m), high Mg# (67.2–75.9), high Ni (200–440 μg/g), and high Cr (470–1,250 μg/g). The following criteria summarized by Velasco-Tapia and Verma (2001) have been proposed for primitive magmas: $FeO^T/MgO < 1$ (Tatsumi et al. 1983); Mg# > 62 and MgO > 6% (Luhr 1997); Mg# > 63 (Green 1971); Mg# = 68–76 (Frey et al. 1978); Ni > 235 μg/g (Sato 1977); $SiO_2 < 50\%$, Mg# > 70, Ni > 400–500 μg/g, and Cr > 1,000 μg/g (Wilson 1989).

The LTVF primitive rocks show relatively uniform isotopic compositions as follows: $(^{87}Sr/^{86}Sr)_i$ 0.70331 ± 0.00015 (1 s; $n = 14$); $(^{143}Nd/^{144}Nd)_i$ 0.51291 ± 0.00007 ($n = 14$); $^{206}Pb/^{204}Pb$ 18.78 ± 0.09 ($n = 11$); $^{207}Pb/^{204}Pb$ 15.57 ± 0.04 ($n = 11$); $^{208}Pb/^{204}Pb$ 38.42 ± 0.15 ($n = 11$), and therefore, for all practical purposes the mantle source can be considered relatively isotopically homogeneous, justifying thus the inverse modelling presented here. The method is the same as that proposed by Hofmann and Feigenson (1983), and was used by Ormerod et al. (1991) for the Big Pine volcanic field, California and by Velasco-Tapia and Verma (2001) for the Sierra de Chichinautzin, Mexico. Both these latter papers reproduced the relevant equations.

The results (the corresponding figure and table are not presented here to comply with space limitations) show that La is the most incompatible element in the LTVF magmas. The somewhat higher incompatibility of La as compared to other incompatible elements is probably consistent with the presence of garnet in the mantle source of these magmas because this mineral (especially pyrope-rich garnet) shows very low mineral/melt partition coefficient for La as compared to Th, U, Nb, Ta, and K (van Westrenen et al. 2001). Furthermore, for the most common mantle mineral olivine the partition coefficient for La is smaller than for K, Rb, Cs, Ba, Sr, Th, U, and Ta (Torres-Alvarado et al. 2003). Therefore, if the bulk partition coefficient of La is to be smaller than for these other incompatible elements, olivine + garnet should dominate in relative abundance over (clino + ortho)pyroxenes in the mantle source region of the LTVF.

The remaining REE (Ce to Lu) are progressively less incompatible than La; similarly, Th, Ba, and Sr, although highly incompatible, are relatively less incompatible than La, and the remaining elements (Cs, K, Zr, Rb, Hf, Ti, and Y) are still less incompatible (plot not shown). Similarly, actual values of slopes and intercepts for $[C^{La}]_E - [C^i]_E$ as well as $[C^{La}]_E$–$[C^{La}/C^i]_E$ linear regressions, along with their respective errors, were also obtained, but are not tabulated.

Instead, from the latter sets of regressions, it is useful to prepare intercept–slope (I^i–m^i) diagrams (Fig. 14), in which

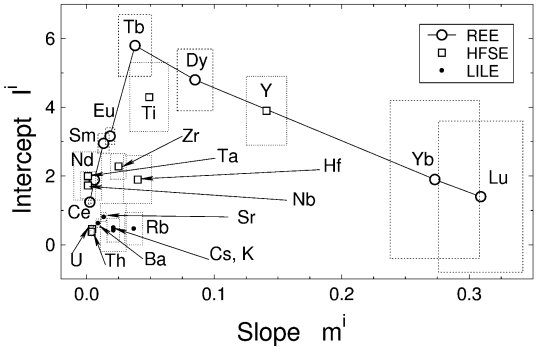

Fig. 14 Diagrams of m^i–I^i (slope–intercept) for the LTVF primitive magmas. The size of each *rectangle* (*dotted* or *dashed lines*) represents one standard error on the regression parameters, derived from the C^{La}/C^i versus C^{La} diagrams (plot not shown). Note LILE (Ba, Cs, K, Rb, and Sr) and HFSE (Nb, Hf, Ta, Zr, and Ti) as well as other incompatible elements (also called HFSE: Th and U; see, e.g. Rollinson 1993), plot below or very close to the REE (Ce–Lu) curve, indicating no significant fractionation between these three groups of elements (LILE, HFSE, and REE). Y plots exactly on the REE curve. If there were a depletion of HFSE as compared to LILE and REE, the HFSE should plot well above the REE curve (see Ormerod et al. 1991)

intercept $I^i = \left(C_0^{La}/C_0^i\right)(1 - P^i)$ and
slope $m^i = \left(D_0^i/C_0^i\right)$,

where $C^i{}_0$ refers to the concentration of element i in the source, $D^i{}_0$ the bulk distribution coefficient for the source prior to melting, and P^i the bulk partition coefficient corresponding to the melting phases.

The slope values increase very slowly from Ce to Tb but much more rapidly from Tb to Lu, whereas the intercept values increase very rapidly from Ce to Tb and then decrease rather slowly from Tb to Lu (Fig. 14). For the LREE (La–Nd) and MREE (Sm–Tb), it appears that $D^i{}_0 \sim 0$ and $(1 - P^i) \sim 1$, so that an increase in intercept means continuously decreasing source concentrations from La (reference element) to Tb (element with the highest intercept; Fig. 14). For Dy and HREE (Yb and Lu), $D^i{}_0$ becomes increasingly significant, giving rise to higher slopes. Elements such as Yb and Lu are likely to be concentrated in garnet, which will constitute a significant proportion of the primary melt norm (Ormerod et al. 1991). Significantly higher slopes for Yb and Lu than the other REE (Fig. 14) suggest the presence of garnet in the source of the LTVF magmas. The very large difference between m^{La} ($=0$ by definition of the regression procedure using La as the reference element) or m^{Ce} (~ 0.0025) and m^{Yb} (~ 0.273) or m^{Lu} (~ 0.309) may also imply a LREE-enriched source, i.e. silicate earth-normalized $[La/Yb]_E$ or $[La/Lu]_E > 1$, although it would be difficult to ascertain this inference because $D^i{}_0$ is susceptible to fluctuations in the source garnet/clinopyroxene ratio (Ormerod et al. 1991).

When the results for other incompatible elements are examined along with the REE data, a systematic pattern emerges (Fig. 14). At low slope values, the intercepts increase rapidly from Th to Ti, which indicates decreasing concentrations of trace elements in the LTVF source from Th to LREE to Ti. All HFS elements (Th, U, Hf, Zr, and Ti) fall below the REE trend for Ce–Tb (Fig. 14). Although the regressions for Nb and Ta were not statistically significant at the 95% confidence level, they have also been plotted, lying close to Ce and Nd (Fig. 14). Note also that HFS element Y (also classified as a REE) falls right on the REE trend between Dy and Yb. These results confirm that the source of the LTVF magmas is not depleted in HFS elements (Zr, Hf, Ti, and Th, including Nb and Ta) in comparison to the LILE (K, Rb, Ce, Ba, and Sr) and LREE (La, Ce, and Nd) or MREE (Sm, Eu, and Tb). Mantle source composition for the LTVF magmas can also be estimated but respective partition coefficients for major mantle minerals (olivine, orthopyroxene, clinopyroxene, and garnet) will have to be assumed. Given the large uncertainties in the literature values for these partition coefficients (Torres-Alvarado et al. 2003), it will be more advisable to experimentally measure these partition coefficients in the LTVF primitive magmas before inferring the LTVF mantle source concentrations.

Finally, it is illustrative to point out that Ormerod et al. (1991), in the Big Pine volcanic field, observed that Nb and Ta (including Zr and Hf) plotted well above their REE curve, in the region of a low to moderate slope combined with a high intercept (i.e. in the upper left corner of the diagram), and they interpreted this finding as consistent with low source abundances of these HFS elements as compared to the REE and LILE in their study area. Velasco-Tapia and Verma (2001) and Verma (2004), on the other hand, obtained similar results (as the LTVF) for the central and eastern parts of the Mexican Volcanic Belt.

Peridotite versus eclogite and lithospheric versus asthenospheric source

The basic and ultrabasic major element compositions of the LTVF rocks (low SiO_2 and high MgO contents) suggest that a purely eclogite source is not suitable for them. Instead, a garnet peridotite source is required. I decided not to use the trace element constraints such as Zr, Hf, and Yb, because of the conflicting partition coefficient data for eclogite and peridotite sources presented by van Westrenen et al. (2001) and Perterman et al. (2004). Geochemical modelling using van Westrenen et al. (2001) data would support a peridotite source whereas Perterman et al. (2004) data would point out an eclogite source, although the latter would be better applicable to more silica-rich magmas than those observed in the LTVF. Furthermore, I note that magmas derived from an eclogite source (recycled subducted slab) should likely show positive Nb anomalies in Figs. 4, 7c, d and Table 3. None of these features is observed for the LTVF magmas. Their relatively high $^{206}Pb/^{204}Pb$ (Fig. 6) might argue for an asthenospheric component (Hawkesworth et al. 1990). In this connection, Wilson and Downes (1991) pointed out that extension-related alkaline magmas in western and central Europe may have, in addition to a lithospheric source, an asthenospheric component represented by HIMU Pb-isotope characteristics.

From relatively high Nb/Y ratios (>3) for Quaternary extension-related alkaline volcanic rocks from Turkey, Alici et al. (2002) inferred an asthenospheric mantle source, whereas high K/Nb and Rb/Nb were taken as indicating a lithospheric mantle source. For the LTVF primitive magmas, Nb/Y is low (<3), ranging from about 0.7 to 2.6 (1.2 ± 0.5; $n = 19$), and K/Nb and Rb/Nb are high, ranging, respectively, from about 130 to 650 (400 ± 140; $n = 19$) and 0.4 to 1.4 (0.8 ± 0.3; $n = 19$). Therefore, although asthenosphere source cannot be ruled out, it appears that the corresponding mantle source is likely to be dominated by the continental lithosphere (trace element evidence). A pressure-released anhydrous melting of such a source, probably aided by the addition of deep fluids, and eruption of magmas facilitated from ongoing rifting or extensional

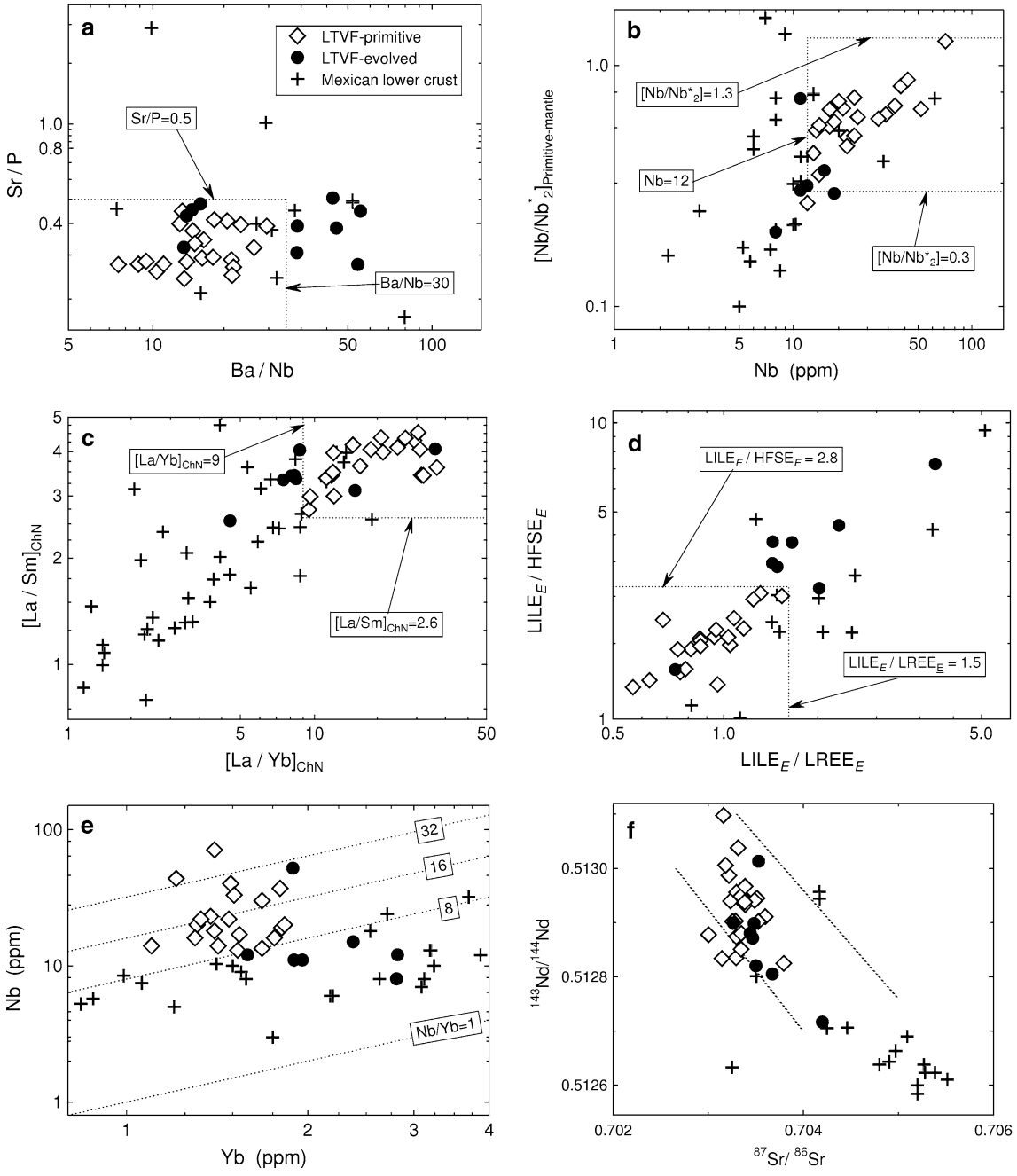

Fig. 15 Selected bivariate diagrams for primitive as well as evolved LTVF rocks. Reference lines are the same as in Figs. 5, 7, and 8 (see these figures for more explanation). Lower crustal rocks from Mexico are plotted to show that the evolved LTVF rocks can be generated through assimilation of crust by primitive magmas. **a** Ba/Nb–Sr/P; **b** Nb–$[Nb/Nb^*_2]_{Primitive\text{-}mantle}$; **c** $(La/Yb)_{ChN}$–$(La/Sm)_{ChN}$; and **d** $[LILE_E/LREE_E]$–$[LILE_E/HFSE_E]$; **e** Yb–Nb; and **f** $^{87}Sr/^{86}Sr$–$^{143}Nd/^{144}Nd$

processes beneath the EAP, along the Gulf of Mexico coastal region, is a viable mechanism for the LTVF.

Nelson et al. (1995) concluded that LTVF ne-normative magmas resulted from variable degrees of melting of the mantle at pressures between 30+ and 20 kbar. The pressure and temperature at which magma segregates from its garnet peridotitic source can also be estimated from the empirical relationships proposed by Albarède (1992) using all primitive rock data, obtaining for the LTVF an average temperature ~1,400 ± 60°C and pressure ~25 ± 9 kbar ($n = 19$). The quoted temperature and pressure uncertainties are simply one standard deviation of all temperature and pressure estimates, respectively, and do not include the inevitable errors associated with the regression procedure which were not reported by Albarède (1992). Similarly, using the model of Wang et al. (2002) based on major element compositions of primary melts pressure estimates for the

LTVF magmas were between about 30 and 40 kbar. Although thickness of the continental lithosphere is not precisely known in Mexico, these pressure estimates may be well within this lithosphere.

Origin of evolved magmas

Nelson et al. (1995) suggested that LTVF ne-normative evolved magmas originated through fractionation of olivine ± clinopyroxene ± plagioclase of more primitive magmas, whereas silica-saturated (hy-normative) magmas might have originated by higher degrees of melting, perhaps under higher water-saturated conditions, the water being supplied by the subducting fluids. They also suggested that the magmas "parental to hy-normative lavas" were generated at lower pressure and/or higher water concentrations than the primitive magmas. They discarded the crust as the only additional (contamination and water-supply) source to explain the chemical and isotopic characteristics of evolved magmas, probably because they considered only the upper continental crust, which is likely to have rather high $^{87}Sr/^{86}Sr$ and low $^{143}Nd/^{144}Nd$ ratios and whose assimilation should significantly increase $^{87}Sr/^{86}Sr$ and decrease $^{143}Nd/^{144}Nd$ of these evolved magmas as compared to the primitive ones.

The main difficulties with the model that evolved LTVF rocks originated from partial melting of the mantle in the presence of fluids from subducted slab proposed by Nelson et al. (1995) are that: (1) the so-called high-Mg basic magmas with "arc-type" characteristics, as assumed by these authors to be "parental" to the evolved magmas, have not been observed in the LTVF; (2) none of the primitive LTVF rocks shows a subduction signature as evidenced in this study (Figs. 5, 7a–f, 8a–c, 13a, b, 14); (3) the isotopic data for any of the LTVF rocks (Figs. 5, 6), whether primitive or evolved, also do not require a subduction component; and (4) the discrimination diagrams (Figs. 9, 10, 11, 12) for all basic rocks (primitive as well as evolved) show a continental rift setting for the LTVF and not an arc setting.

Nelson et al. (1995) preferred a three-component model (mantle, subduction fluids, and crust) although the requirement of subduction fluids was not clearly shown, because crust alone, particularly the lower crust, would provide the necessary assimilant to explain all the chemical and isotopic characteristics of the LTVF magmas. If mafic lower crust was involved in the genesis of the LTVF magmas, the characteristics of evolved magmas can be easily explained by contamination of primitive magmas by such a heterogeneous crust. To illustrate this possibility, Fig. 15a–f shows that the LTVF-evolved rocks plot between the primitive rocks and widely varying Mexican lower crustal compositions. The Mexican lower crust is highly heterogeneous as is the lower crust from elsewhere (Weaver and Tarney 1984; Taylor and McLennan 1985; Rudnick 1992; Chen and Arculus 1995). The REE characteristics of evolved rocks are consistent with such a mixing process (Fig. 15c), and the same is true for other trace elements (Fig. 15a, b, d, e) and Sr and Nd isotopic compositions (Fig. 15f).

Therefore, it is likely that the evolved alkaline and sub-alkaline rocks also originated from a similar mantle source perhaps at shallower levels than the primitive rocks, but they underwent crustal assimilation or assimilation coupled with fractional crystallization before eruption. No modelling is really required, at this stage, to be included in Fig. 15 because it is graphically clear that an assimilation of lower crust can explain the chemical and isotopic differences between the LTVF primitive and evolved rocks. Partial melting of mafic lower crust by periodic influx of basic magma and mixing of these magmas is a viable mechanism for the LTVF both from geochemical (Fig. 15) and thermal considerations (Wilcox 1999; Petford and Gallahar 2001). Mafic assimilant will not drastically change the major element compositions of the LTVF magmas. The lower crust, rather than the upper crust, is more likely because of the similarities of Sr, Nd, and Pb isotope data for evolved and primitive rocks. Unfortunately, the involvement of lower crust cannot at present be tested for Pb isotopes because no such data are still available for the Mexican lower crust.

Tectonic considerations

If subduction fluids from the "sub-horizontal" Cocos plate were not involved in the origin of the LTVF magmas, the reason for this non-involvement may have to be explained. Thus, the absence of a clear subduction signal in basic rocks from the LTVF may mean that the slab-derived fluids, whether dominantly from subducted sediments (Plank and Langmuir 1993), from altered oceanic crust (Hawkesworth et al. 1991), or from lower oceanic crust (Ernst 1999), are released too close to the trench and probably too shallow to cause mantle melting. In South America, diminution or even cessation of subduction-related volcanism during mid-late Tertiary has been observed and is interpreted to be associated to a sub-horizontal slab (e.g. Kay et al. 1987).

Nelson et al. (1995) argued that the LTVF may represent an unusual setting where both arc- as well as back-arc rocks lie in the same geographical region. However, the so-called "arc" rocks by Nelson et al. (1995) are simply evolved rocks, whose origin can be explained by the incorporation of a lower crustal component (Fig. 15). Therefore, no truly "arc-type" (subduction-related) rocks are present in the LTVF. Furthermore, I am at a loss to understand how such an unusual tectonic setting—"back-arc"—is geometrically feasible. As its name suggests, a "back-arc" should lie geographically behind the contemporaneous "arc", i.e. in a region farther away from the trench. In other words, there must be at least some geographical distinction

between them—the arc should lie somewhat closer to the trench than the corresponding back-arc.

On the other hand, one may argue that the LTVF magmas are chemically similar to those erupting in the back-arc region of other arcs (some back-arc rocks do plot in the field of LTVF rocks in Figs. 7, 13) and, therefore, the LTVF magmatism should be called back-arc magmatism. Then, we should be able to actually locate the arc between the LTVF and the trench, which is simply not possible because there is no late Miocene to Recent volcanism (of an age similar to the LTVF) between the LTVF and the trench (Fig. 1). I conclude that, geometrically speaking, the existence of a back-arc without an arc cannot be true. None of these terminologies seems appropriate to describe the LTVF. We should, therefore, possibly accept a less orthodox explanation, such as the absence of subduction-related volcanism in the LTVF. This will be an entirely feasible conclusion in view of the "sub-horizontal" nature of the downgoing slab corresponding to the LTVF. Furthermore, consistent with Robin and co-workers (Robin 1976, 1982b; Robin and Tournon 1978; Cantagrel and Robin 1979), the LTVF may well belong to the north–south trending Miocene to Recent EAP (Fig. 1) with abundant alkaline rocks, whose origin might be related to the extensional tectonics along the Gulf of Mexico coastal region. This extension may not be related to the current subduction of the Cocos plate, but probably similar to the extension envisioned for the central part of the Mexican Volcanic Belt (Márquez et al. 2001). The absence of "true" subduction-related volcanism (Verma 2002; this work), the extensional nature of earthquakes (Singh and Pardo 1993), and the absence of a fore-arc basin (von Huene 1989) in southern Mexico may be consistent with the location of the back-arc (without an arc!) in the region of the Balsas basin (between the LTVF and the MAT in Fig. 1; see also Verma 2004). The origin of the EAP, including the LTVF, can thus be visualized as largely independent of the current subduction of the Cocos plate beneath Mexico.

Conclusions

In the LTVF primitive basanite and alkali basalt magmas are abundant. The distribution of rock types is very similar to that in well-known rifts such as Djibouti and Rio Grande or extension-related areas such as E and NE China and western USA. The Sr, Nd, and Pb isotopic ratios for the LTVF magmas show the following ranges: $^{87}Sr/^{86}Sr$ 0.70300–0.70420; $^{143}Nd/^{144}Nd$ 0.51271–0.51310; $^{206}Pb/^{204}Pb$ 18.62–18.92; $^{207}Pb/^{204}Pb$ 15.47–15.65; $^{208}Pb/^{204}Pb$ 38.06–38.64.

Their trace element patterns (HFSE, REE, and LILE characteristics) are similar to those of well-known rifts and extension-related areas. Inverse modelling of geochemical data for the LTVF primitive rocks points to a source enriched in highly incompatible elements (LILE and LREE), including the HFSE. The basanitic and alkaline basaltic magmas probably originated from a deep-seated (~30 kbar) garnet peridotite lithospheric (and less likely, asthenospheric?) source(s), but without a significant contribution from the downgoing Cocos plate. It is also concluded that the LTVF evolved magmas too do not require a slab component in their genesis. The continental crust, particularly the lower crust, provides the complementary reservoir to explain the origin of evolved rocks from more primitive magmas.

I propose that a general shift towards the right of the mantle array on a conventional Sr–Nd isotope diagram (here termed as "Sr-shift") is a strong criterion for distinguishing arc magmas from those from a rift or extensional setting. Finally, low values of the combined normalized parameters [$LILE_E/LREE_E$] and [$LILE_E/(HFSE_E$] are shown to be excellent indicators of a rift environment as is the case of the LTVF, whereas their high values are diagnostic of an arc setting.

The Nb anomaly, quantitatively defined in this work either with respect to Th and K or with respect to Ba and La, when used with other slab- or mantle-sensitive parameters can provide a useful framework to distinguish between arc and rift tectonic settings. In fact, a synthesis of statistical parameters for Nb anomaly clearly shows that, in terms of this important parameter, the LTVF basic and ultrabasic rocks are similar to numerous rifts and extension and continental break-up regions but totally distinct from *all* arcs compiled in the present study. I suggest that rifts, extension-related areas and continental break-up regions with a positive Nb anomaly have a significant contribution from the asthenosphere, whereas extensional regions showing a negative Nb anomaly are dominated by the lithospheric sources.

Acknowledgements I am grateful to: Al Hofmann and B. Schultz Dobrich for use of experimental facilities at the Max-Planck-Institut für Chemie and Universität Mainz, respectively; Marcos Milán for accompanying me during sample collection from the Los Tuxtlas volcanic field; Alexander von Humboldt Foundation for support to carry out the analytical work in Germany; and H. Downes, two anonymous reviewers, one of them persistently provided (at two occasions) extensive thought-provoking critical comments, the editor Kaj Hoernle, and the editor-in-chief Wolf-Christian Dullo for constructive comments on earlier versions of this paper. I also thank Seth Sadofsky and Kaj Hoernle for sharing their unpublished data from subducting Cocos plate to be included in Fig. 6 of the present paper.

References

Agrawal S, Guevara M, Verma SP (2004) Discriminant analysis applied to establish major element field boundaries for tectonic varieties of basic rocks. Int Geol Rev 46:575–594

Albarède F (1983) Inversion of batch melting equations and the trace element pattern of the mantle. J Geophys Res 88:10573–10583

Albarède F (1992) How deep do common basaltic magmas form and differentiate? J Geophys Res 97:10997–11009

Alici P, Temel A, Gourgaud A (2002) Pb–Nd–Sr isotope and trace element geochemistry of Quaternary extension-related alkaline

volcanism: a case study of Kula region (western Anatolia, Turkey). J Volcanol Geotherm Res 115:487–510
Aoki K-I, Yoshida T, Yusa K, Nakamura Y (1985) Petrology and geochemistry of the Nyamuragira volcano, Zaire. J Volcanol Geotherm Res 25:1–28
Arculus RJ (1976) Geology and geochemistry of the alkali basalt–andesite association of Grenada, Lesser Antilles island arc. Geol Soc Am Bull 87: 612–624
Auchapt A, Dupuy C, Dostal J, Kanika M (1987) Geochemistry and petrogenesis of rift-related volcanic rocks from South Kivi (Zaire). J Volcanol Geotherm Res 31:33–46
Barberi F, Ferrara G, Santacroce R, Treuil M, Varet J (1975) A transitional basalt-pantellerite sequence of fractional crystallization, the Boina centre (Afar rift, Ethiopia). J Petrol 16:22–56
Barrat JA, Joron JL, Taylor RN, Fourcade S, Nesbitt RW, Jahn BM (2003) Geochemistry of basalts from Manda Hararo, Ethiopia: LREE-depleted basalts in Central Afar. Lithos 69:1–13
Barsdell M (1988) Petrology and petrogenesis of clinopyroxene-rich tholeiitic lavas, Merelava volcano, Vanuatu. J Petrol 29:927–964
Barsdell M, Berry RF (1990) Origin and evolution of primitive island arc ankaramites from western Epi, Vanuatu. J Petrol 31:747–777
Basu AR, Junwen W, Wankang H, Guanghong X, Tatsumoto M (1991) Major element, REE, and Pb, Nd and Sr isotopic geochemistry of Cenozoic volcanic rocks of eastern China: implications for their origin from suboceanic-type mantle reservoirs. Earth Planet Sci Lett 105:149–169
Bau M, Knittel U (1993) Significance of slab-derived partial melts and aqueous fluids for the genesis of tholeiitic and calc-alkaline island-arc basalts: evidence from Mt. Arayat, Philippines. Chem Geol 105:233–251
Bell K, Peterson T (1991) Nd and Sr isotopic systematics of Shombole volcano, East Africa, and the links between nephelinites, phonolites, and carbonatites. Geology 19:582–585
Besch T, Verma SP, Krammer U, Negendank JFW, Tobschall HJ, Emmermann R (1995) Assimilation of sialic crustal material by volcanics of the easternmost extension of the Trans-Mexican Volcanic Belt—evidence from Sr and Nd isotopes. Geofis Int 34:263–281
Bloomer SH, Stern RJ, Fisk E, Geschwind CH (1989) Shoshonitic volcanism in the northern Mariana arc. 1. Mineralogic and major and trace element characteristics. J Geophys Res 94:4469–4496
Borg LE, Clynne MA, Bullen TD (1997) The variable role of slab-derived fluids in the generation of a suite of primitive calc-alkaline lavas from the southernmost Cascades, California. Can Miner 35:425–452
Brewer TS, Hergt JM, Hawkesworth CJ, Rex D, Storey BC (1992) Coats Land dolerites and the generation of Antarctic continental flood basalts. In: Storey BC, Alabaster T, Pankhurst RJ (eds) Magmatism and the causes of continental break-up. Geol Soc Spec Publ 68:185–208
Brophy JG (1986) The Cold Bay volcanic center, Aleutian volcanic arc. I. Implications for the origin of hi-alumina arc basalt. Contrib Mineral Petrol 93:368–380
Brown GM, Holland JG, Sigurdsson H, Tomblin JF, Arculus RJ (1977) Geochemistry of the Lesser Antilles volcanic island arc. Geochim Cosmochim Acta 41:785–801
Bryan WB, Stice GD, Ewart A (1972) Geology, petrography, and geochemistry of the volcanic islands of Tonga. J Geophys Res 77:1566–1585
Burbach GV, Frohlich C, Pennington WD, Matumoto T (1984) Seismicity and tectonics of the subducted Cocos plate. J Geophys Res 89:7719–7735
Butler JC, Woronow A (1986) Discrimination among tectonic settings using trace element abundances of basalts. J Geophys Res 91:10289–10300
Cabanis B, Lecolle M (1989) Le diagramme La/10-Y/15-Nb/8: un outil pour la discrimination des séries volcaniques et la mise en évidence des processus de mélange et/ou de contamination crustale. CR Acad Sci Paris 309:2023–2029
Camp VE, Roobol MJ, Hooper PR (1991) The Arabian continental alkali basalt province: part II. Evolution of Harrats Khaybar, Ithnayn, and Kura, Kingdom of Saudi Arabia. Geol Soc Am Bull 103:363–391
Cantagrel J-M, Robin C (1979) K–Ar dating on eastern Mexican volcanic rocks—relations between the andesitic and the alkaline provinces. J Volcanol Geotherm Res 5:99–114
Carr MJ, Rose WI, Stoiber RE (1982) Central America. In: Thorpe RS (ed) Andesites. Wiley, Chichester, pp 149–166
Carr MJ, Feigenson MD, Bennett EA (1990) Incompatible element and isotopic evidence for tectonic control of source mixing and melt extraction along the Central American arc. Contrib Mineral Petrol 105:369–380
Carrasco-Núñez G (2000) Structure and proximal stratigraphy of Citlaltépetl volcano (Pico de Orizaba), Mexico. In: Delgado-Granados H, Aguirre-Díaz G, Stock JM (eds) Cenozoic tectonics and volcanism of Mexico. Geol Soc Am Spec Pap 334:247–262
Chauvel C, Jahn B-M (1984) Nd–Sr isotope and REE geochemistry of alkali basalts from the Massif Central, France. Geochim Cosmochim Acta 48:93–110
Chen W, Arculus RJ (1995) Geochemical and isotopic characteristics of lower crustal xenoliths, San Francisco volcanic field, Arizona, U.S.A. Lithos 36:203–225
Chung S-L, Sun SS, Tu K, Chen-Hong C, Lee CL (1994) Late Cenozoic basaltic volcanism around the Taiwan Strait, SE China: product of lithosphere–asthenosphere interaction during continental extension. Chem Geol 112:1–20
Chung SL, Jahn BM, Chen SJ, Lee T, Chen C-H (1995) Miocene basalts in northwestern Taiwan: evidence for EM-type mantle sources in the continental lithosphere. Geochim Cosmochim Acta 59:549–555
Class C, Altherr R, Volker F, Eberz G, McCulloch MT (1994) Geochemistry of Pliocene to Quaternary alkali basalts from the Huri Hills, northern Kenya. Chem Geol 113:1–22
Davidson J (1985) Mechanisms of contamination in Lesser Antilles island arc magmas from radiogenic and oxygen isotope relationships. Earth Planet Sci Lett 72:163–174
Davidson JP (1986) Isotopic and trace element constraints on the petrogenesis of subduction-related lavas from Martinique, Lesser Antilles. J Geophys Res 91:5943–5962
Davidson JP (1996) Deciphering mantle and crustal signatures in subduction zone magmatism. In: Bebout GE, Scholl DW, Kirby SH, Platt JP (eds) Subduction top to bottom. AGU Geophys Monogr 96:251–268
Davidson JP, Wilson IR (1989) Evolution of an alkali basalt-trachyte suite from Jebel Marra volcano, Sudan, through assimilation and fractional crystallization. Earth Planet Sci Lett 95:141–160
Davies JH, Stevenson DJ (1992) Physical model of source region of subduction zone volcanics. J Geophys Res 97:2037–2070
Defant MJ, Drummond MS (1990) Derivation of some modern arc magmas by melting of young subducted lithosphere. Nature 347:662–665
Defant MJ, Jacques D, Maury RC, De Boer J, Joron J-L (1989) Geochemistry and tectonic setting of the Luzon arc, Philippines. Geol Soc Am Bull 101:663–672
Defant MJ, Maury RC, Ripley EM, Feigenson MD, Jacques D (1991a) An example of island-arc petrogenesis: geochemistry and petrology of the southern Luzon arc, Philippines. J Petrol 32:455–500
Defant MJ, Richerson PM, De Boer JZ, Stewart RH, Maury RC, Bellon H, Drummond MS, Feigenson MD, Jackson TE (1991b) Dacite genesis via both slab melting and differentiation: petrogenesis of La Yeguada volcanic complex, Panama. J Petrol 32:1101–1142
Defant MJ, Sherman S, Maury RC, Bellon H, de Boer J, Davidson J, Kepezhinskas P (2001) The geology, petrology, and petrogenesis of Saba Island, Lesser Antilles. J Volcanol Geotherm Res 107:87–111
Demant A (1981) L'axe néo-volcanique transmexicain, étude volcanologique et pétrographique, signification géodynamique. Doctoral thesis, Faculté des Sciences et Techniques de St. Jérome, vol. Université de Droit, d'Economie et des Sciences d'Aix-Marseille, 259 pp

De Mulder M, Hertogen J, Deutsch S, André L (1986) The role of crustal contamination in the potassic suite of the Karisimbi volcano (Virunga, African Rift Valley). Chem Geol 57:117–136

Deniel C, Vidal P, Coulon C, Vellutini P, Piguet P (1994) Temporal evolution of mantle sources during continental rifting: the volcanism of Djibouti (Afar). J Geophys Res 99:2853–2869

DePaolo DJ, Johnson RW (1979) Magma genesis in the New Britain island-arc: constraints from Nd and Sr isotopes and trace-element patterns. Contrib Mineral Petrol 70:367–379

DePaolo DJ, Wasserburg GJ (1976) Nd isotopic variations and petrogenetic models. Geophys Res Lett 3:249–252

Deruelle B (1982) Petrology of the Plio-Quaternary volcanism of the south-central and meridional Andes. J Volcanol Geotherm Res 14:77–124

Devey CW, Stephens WE (1992) Deccan-related magmatism west of the Seychelles–India rift. In: Storey BC, Alabaster T, Pankhurst RJ (eds) Magmatism and the causes of continental break-up. Geol Soc Spec Publ 68:271–291

Devine JD (1995) Petrogenesis of the basalt–andesite–dacite association of Grenada, Lesser Antilles island arc, revisited. J Volcanol Geotherm Res 69:1–33

Duncan AR, Erlank AJ, Marsh JS (1984) Regional geochemistry of the Karoo igneous province. Spec Publ Geol Soc S Afr 13:355–388

Duncker KE, Wolff JA, Harmon RS, Leat PT, Dickin AP, Thompson RN (1991) Diverse mantle and crustal components in lavas of the NW Cerros del Rio volcanic field, Rio Grande Rift, New Mexico. Contrib Mineral Petrol 108:331–345

Dupuy C, Dostal J, Marcelot G, Bougault H, Joron JL, Treuil M (1982) Geochemistry of basalts from central and southern New Hebrides arc: implication for their source rock composition. Earth Planet Sci Lett 60:207–225

Edwards CMH, Menzies MA, Thirlwall MF, Morris JD, Leeman WP, Harmon RS (1994) The transition to potassic alkaline volcanism in Island arcs: the Ringgit-Beser complex, east Java, Indonesia. J Petrol 35:1557–1595

Elliott T, Plank T, Zindler A, White WM, Bourdon B (1997) Element transport from slab to volcanic front at the Mariana arc. J Geophys Res 102:14991–15019

Ernst WG (1999) Hornblende, the continent maker: evolution of H_2O during Circum-Pacific subduction versus continent collision. Geology 27:675–678

Ewart A, Brothers RN, Mateen A (1977) An outline of the geology and geochemistry, and the possible petrogenetic evolution of the volcanic rocks of the Tonga-Kermadec-New Zealand island arc. J Volcanol Geotherm Res 2:205–270

Fan Q, Hooper PR (1991) The Cenozoic basaltic rocks of eastern China: petrology and chemical composition. J Petrol 32:765–810

Faure G (1986) Principles of isotope geology, 2nd edn. Wiley, New York, 653 pp

Feigenson MD, Carr MJ (1986) Positively correlated Nd and Sr isotope ratios of lavas from the Central America volcanic front. Geology 14:79–82

Ferriz H, Mahood GA (1987) Strong compositional zonation in a silicic magmatic system: Los Humeros, Mexican Neovolcanic Belt. J Petrol 28:171–209

Fisk MR (1986) Basalt magma interaction with harzburgite and the formation of high-magnesium andesite. Geophys Res Lett 13:467–470

Fitton JG, James D, Leeman WP (1991) Basic magmatism associated with Late Cenozoic extension in the western United States: compositional variations in space and time. J Geophys Res 96:13693–13711

Foden JD, Varne R (1980) The petrology and tectonic setting of Quaternary–Recent volcanic centres of Lombok and Sumbawa, Sunda arc. Chem Geol 30:210–226

Frey FA, Green DH, Roy SD (1978) Integrated models of basalt petrogenesis: a study of quartz tholeiites to olivine melilitites from south eastern Australia utilizing geochemical and experimental petrological data. J Petrol 19:463–513

Frey FA, Gerlach DC, Hickey RL, Lopez-Escobar L, Munizaga-Villavicencio F (1984) Petrogenesis of the Laguna del Maule volcanic complex, Chile (36°S). Contrib Mineral Petrol 88:133–149

Friedländer I, Sonder RA (1923) Über das Vulkangebeit von San Martin Tuxtla im Mexiko. Zeitschr f Vulkanol VII:162–187

Gamble JA, Wright IC, Woodhead JD, McCulloch MT (1995) Arc and back-arc geochemistry in the southern Kermadec arc–Ngatoro basin and offshore Taupo volcanic zone, SW Pacific. In: Smellie JL (ed) Volcanism associated with extension at consuming plate margins. Geol Soc Spec Publ 81:193–212

Gerlach DC, Frey FA, Moreno-Roa H, Lopez-Escobar L (1988) Recent volcanism in the Puyehue-Cordon Caulle region, southern Andes, Chile (40.5°S): petrogenesis of evolved lavas. J Petrol 29:333–382

Gibson SA, Thompson RN, Leat PT, Dickin AP, Morrison MA, Hendry GL, Mitchell JG (1992) Asthenosphere-derived magmatism in the Rio Grande rift, western USA: implications for continental break-up. In: Storey BC, Alabaster T, Pankhurst RJ (eds) Magmatism and the causes of continental break-up. Geol Soc Spec Publ 68:61–89

Gómez-Tuena A, LaGatta AB, Langmuir CH, Goldstein SL, Ortega-Gutiérrez F, Carrasco-Núñez G (2003) Temporal control of subduction magmatism in the eastern Trans-Mexican Volcanic Belt: mantle sources, slab contributions, and crustal contamination. G3 Geochem Geophys Geosys 4:8912. DOI 10.1029/2003GC000524

Graham DW, Zindler A, Kurz MD, Jenkins WJ, Batiza R, Staudigel H (1988) He, Pb, Sr and Nd isotope constraints on magma genesis and mantle heterogeneity beneath young Pacific seamounts. Contrib Mineral Petrol 99:446–463

Green DH (1971) Composition of basaltic magmas as indicators of conditions of origin: application to oceanic volcanism. Phil Trans R Soc London 268A:707–725

Han B-f, Wang S-g, Kagami H (1999) Trace element and Nd–Sr isotope constraints on origin of the Chifeng flood basalts, North China. Chem Geol 155:187–199

Harry DL, Green NL (1999) Slab dehydration and basalt petrogenesis in subduction systems involving very young oceanic lithosphere. Chem Geol 160:309–333

Hart SR (1984) A large-scale isotope anomaly in the Southern Hemisphere mantle. Nature 309:753–757

Hart WK, WoldeGabriel G, Walter RC, Mertzman SA (1989) Basaltic volcanism in Ethiopia: constraints on continental rifting and mantle interactions. J Geophys Res 94:7731–7748

Hawkesworth CJ, Gallagher K (1992) Paraná magmatism and the opening of the South Atlantic. In: Storey BC, Alabaster T, Pankhurst RJ (eds) Magmatism and the causes of continental break-up. Geol Soc Spec Publ 68:221–240

Hawkesworth CJ, O'Nions RK, Pankhurst RJ, Hamilton PJ, Evensen EM (1977) A geochemical study of island-arc and back-arc tholeiites from the Scotia sea. Earth Planet Sci Lett 36:153–162

Hawkesworth CJ, O'Nions RK, Arculus RJ (1979) Nd and Sr isotope geochemistry of island arc volcanics, Grenada, Lesser Antilles. Earth Planet Sci Lett 45:237–248

Hawkesworth CJ, Kempton PD, Rogers NW, Ellam RM, van Calsteren PW (1990) Continental mantle lithosphere, and shallow level enrichment processes in the Earth's mantle. Earth Planet Sci Lett 96:256–268

Hawkesworth CJ, Hergt JM, McDermott F, Ellam RM (1991) Destructive margin magmatism and the contributions from the mantle wedge and subducted crust. Aust J Earth Sci 38:577–594

Hegner E, Smith IEM (1992) Isotopic compositions of late Cenozoic volcanics from southeast Papua New Guinea: evidence for multi-component sources in arc and rift environments. Chem Geol 97:233–249

Heinrich W, Besch T (1992) Thermal history of the upper mantle beneath a young back-arc extensional zone: ultramafic xenoliths from San Luis Potosí, central Mexico. Contrib Mineral Petrol 111:126–142

Hickey RL, Frey FA, Gerlach DC, Lopez-Escobar L (1986) Multiple sources for basaltic arc rocks from the southern volcanic zone of the Andes (34°–41°S): trace element and isotopic evidence for contributions from subducted oceanic crust, mantle, and continental crust. J Geophys Res 91:5963–5983

Hickey-Vargas R, Moreno Roa H, Lopez Escobar L, Frey FA (1989) Geochemical variations in Andean basaltic and silicic lavas from the Villarrica-Lanin volcanic chain (39.5°S): an evaluation of source heterogeneity, fractional crystallization and crustal assimilation. Contrib Mineral Petrol 103:361–386

Hofmann AW, Feigenson MD (1983) Case studies on the origin of basalt. I. Theory and reassessment of Grenada basalts. Contrib Mineral Petrol 84:382–389

Hofmann AW, Feigenson MD, Raczek I (1984) Case studies on the origin of basalt: III. Petrogenesis of the Mauna Ulu eruption, Kilauea, 1969–1971. Contrib Mineral Petrol 88:24–35

Hofmann AW, Jochum KP, Seufert M, White WM (1986) Nb and Pb in oceanic basalts: new constraints on mantle evolution. Earth Planet Sci Lett 79:33–45

Hole MJ, Saunders AD, Marriner GF, Tarney J (1984) Subduction of pelagic sediments: implications for the origin of Ce-Anomalous basalts from the Marianas Islands. J Geol Soc Lond 141:453–472

Holm PM, Hald N, Nielsen TFD (1992) Contrasts in composition and evolution of Tertiary CFBs between West ad East Greenland and their relations to the establishment of the Icelandic mantle plume. In: Storey BC, Alabaster T, Pankhurst RJ (eds) Magmatism and the causes of continental break-up. Geol Soc Spec Publ 68:349–362

Hoogewerff JA, van Bergen MJ, Vroon PZ, Hertogen J, Wordel R, Sneyers A, Nasution A, Varekamp JC, Moens HLE, Mouchel D (1997) U-series, Sr–Nd–Pb isotope and trace-element systematics across an active island arc-continent collision zone: implications for element transfer at the slab–wedge interface. Geochim Cosmochim Acta 61:1057–1072

Hooper PR (1988) The Columbia River basalt. In: Macdougall JD (ed) Continental flood basalts. Kluwer Academic, New York, pp 1–33

Hsu C-N, Chen J-C, Ho K-S (2000) Geochemistry of Cenozoic volcanic rocks from Kirin Province, northeast China. Geochem J 34:33–58

von Huene R (1989) The Middle America convergent plate boundary, Guatemala. In: Winterer EL, Hussong DM, Decker RW (eds) The Eastern Pacific Ocean and Hawaii. The geology of North America. Boulder, Colorado, pp 535–550

Ionov DA, Hofmann AW, Shimizu N (1994) Metasomatism-induced melting in mantle xenoliths from Mongolia. J Petrol 35:753–785

Jochum KP, Verma SP (1996) Extreme enrichment of Sb, Tl and other trace elements in altered MORB. Chem Geol 130:289–299

Johnson CM, Lipman PW (1988) Origin of metaluminous and alkaline volcanic rocks of the Latir volcanic field, northern Rio Grande rift, New Mexico. Contrib Mineral Petrol 100:107–128

Kay RW (1978) Aleutian magnesian andesites: melts from subducted Pacific ocean crust. J Volcanol Geotherm Res 4:117–132

Kay RW, Gast PW (1973) The rare earth content and origin of alkali-rich basalts. J Geol 81:653–682

Kay SM, Gordillo CE (1994) Pocho volcanic rocks and the melting of depleted continental lithosphere above a shallowly dipping subduction zone in the central Andes. Contrib Mineral Petrol 117:25–44

Kay SM, Kay RW (1994) Aleutian magmas in space and time. In: Plafker G, Berg HC (eds) Geology of North America, vol G-1. Geol Soc Am, USA, pp 687–722

Kay SM, Kay RW, Citron GP (1982) Tectonic controls on tholeiitic and calc-alkaline magmatism in the Aleutian arc. J Geophys Res 87:4051–4072

Kay SM, Maksaev V, Moscoso R, Mpodozis C, Nasi C (1987) Probing the evolving Andean lithosphere: mid-late Tertiary magmatism in Chile (29°–30°30′S) over the modern zone of subhorizontal subduction. J Geophys Res 92:6173–6189

Kay SM, Maksaev V, Moscoso R, Mpodozis C, Nasi C, Gordillo CE (1988) Tertiary Andean magmatism in Chile and Argentina between 28°S and 33°S: correlation of magmatic chemistry with a changing Benioff zone. J South Am Earth Sci 1:21–38

Kay SM, Ramos VA, Marquez M (1993) Evidence in Cerro Pampa volcanic rocks for slab-melting prior to ridge-trench collision in southern South America. J Geol 101:703–714

Kempton PD, Fitton JG, Hawkesworth CJ, Ormerod DS (1991) Isotopic and trace element constraints on the composition and evolution of the lithosphere beneath the Southwestern United States. J Geophys Res 96:13713–13735

Kepezhinskas P (1995) Diverse shoshonite magma series in the Kamchatka arc: relationships between intra-arc extension and composition of alkaline magmas. In: Smellie JL (ed) Volcanism associated with extension at consuming plate margins. Geol Soc Spec Publ 81:249–264

Kepezhinskas P, McDermott F, Defant MJ, Hochstaedter A, Drummond MS, Hawkesworth CJ, Koloskov A, Maury RC, Bellon H (1997) Trace element and Sr–Nd–Pb isotopic constraints on a three-component model of Kamchatka arc petrogenesis. Geochim Cosmochim Acta 61:577–600

Kimura J-I, Tanji T, Yoshida T, Iizumi S (2001) Geology and geochemistry of lavas at Nekoma volcano: implications for origin of Quaternary low-K andesite in the north-eastern Honshu arc, Japan. Island Arc 10:116–134

Kita I, Yamamoto M, Asakawa Y, Nakagawa M, Taguchi S, Hasegawa H (2001) Contemporaneous ascent of within-plate type and island-arc type magmas in the Beppu-Shimabara graben system, Kyushu island, Japan. J Volcanol Geotherm Res 111:99–109

Klitgord KD, Mammerickx J (1988) Northern East Pacific Rise: magnetic anomaly and bathymetric framework. J Geophys Res 87:6725–6750

Knittel U, Hegner E, Bau M, Satir M (1997) Enrichment processes in the sub-arc mantle: a Sr–Nd–Pb isotopic and REE study of primitive arc basalts from the Philippines. Can Mineral 35:327–346

Kostopoulos DK (1991) Melting of the shallow upper mantle: a new perspective. J Petrol 32:671–699

Kostopoulos DK, James SD (1992) Parameterization of the melting regime of the shallow upper mantle and the effects of variable lithospheric stretching on mantle modal stratification and trace-element concentrations in magmas. J Petrol 33:665–691

Kudo AM, Jackson ME, Husler JW (1985) Phase chemistry of recent andesite, dacite, and rhyodacite of volcan Pico de Orizaba, Mexican Volcanic Belt: evidence for xenolitic contamination. Geofís Int 24: 679–689

Lassiter JC, DePaolo DJ, Mahoney JJ (1995) Geochemistry of the Wrangellia Flood Basalt Province: implications for the role of continental and oceanic lithosphere in Flood Basalt genesis. J Petrol 36:983–1009

Le Bas MJ (2000) IUGS reclassification of the high-Mg and picritic volcanic rocks. J Petrol 41:1467–1470

Le Bas MJ, Le Maitre RW, Streckeisen A, Zanettin B (1986) A chemical classification of volcanic rocks based on the total alkali-silica diagram. J Petrol 27:745–750

Le Roex AP, Späth A, Zartman RE (2001) Lithospheric thickness beneath the southern Kenya rift: implications from basalt geochemistry. Contrib Mineral Petrol 142:89–106

Lin PN, Stern RJ, Morris J, Bloomer SH (1990) Nd- and Sr-isotopic compositions of lavas from the northern Mariana and southern Volcano arcs: implications for the origin of island arc melts. Contrib Mineral Petrol 105:381–392

Liu C-Q, Masuda A, Xie G-H (1992) Isotope and trace-element geochemistry of alkali basalts and associated megacrysts from the Huangyishan volcano, Kuandian, Liaoning, NE China. Chem Geol 97:219–231

Liu C-Q, Masuda A, Xie G-H (1994) Major- and trace-element compositions of Cenozoic basalts in eastern China: petrogenesis and mantle source. Chem Geol 114:19–42

Lomnitz C (1982) Direct evidence of a subducted plate under southern Mexico. Nature 296:235–238

López-Escobar L, Kilian R, Kempton PD, Tagiri M (1993) Petrography and geochemistry of Quaternary rocks from the southern volcanic zone of the Andes between 41°30′ and 46°00′S, Chile. Rev Geol Chile 20:33–35

Luhr JF (1997) Extensional tectonics and the diverse primitive volcanic rocks in the western Mexican Volcanic Belt. Can Miner 35:473–500

Luhr JF, Aranda-Gómez JJ, Housh TB (1995) San Quintín volcanic field, Baja California Norte, México: geology, petrology, and geochemistry. J Geophys Res 100:10353–10380

Lum CCL, Leeman WP, Foland KA, Kargel JA, Fitton JG (1989) Isotopic variations in continental basaltic lavas as indicators of mantle heterogeneity: examples from the western U.S. Cordillera. J Geophys Res 94:7871–7884

Maaløe S (1994) Estimation of the degree of partial melting using concentration ratios. Geochim Cosmochim Acta 58:2519–2525

Macdonald R, Davies GR, Upton BGJ, Denkley PN, Smith M, Leat PT (1995) Petrogenesis of Silali volcano, Gregory rift, Kenya. J Geol Soc London 152:703–720

Macdonald R, Rogers NW, Fitton JG, Black S, Smith M (2001) Plume-lithosphere interactions in the generation of the basalts of the Kenya rift, East Africa. J Petrol 42:877–900

Márquez A, Oyarzun R, de Ignacio C, Doblas M (2001) Southward migration of volcanic activity in the central Mexican Volcanic Belt: asymmetric extension within a two-layer crustal stretching model. J Volcanol Geotherm Res 112:175–187

Marsh JS (1987) Basalt geochemistry and tectonic discrimination within continental flood basalt provinces. J Volcanol Geotherm Res 32:35–49

Marzoli A, Melluso L, Morra V, Renne PR, Sgrosso I, D'Antonio M, Duarte Morais L, Morais EAA, Ricci G (1999) Geochronology and petrology of Cretaceous basaltic magmatism in the Kwanza basin (western Angola), and relationships with the Paraná-Etendeka continental flood basalt province. J Geodyn 28:341–356

McCulloch MT, Gamble JA (1991) Geochemical and geodynamical constraints on subduction zone magmatism. Earth Planet Sci Lett 102:358–374

McDonough WF, Sun S-S (1995) The composition of the Earth. Chem Geol 120:223–253

McKenzie D, Bickle MJ (1988) The volume and composition of melt generated by extension of the lithosphere. J Petrol 29:625–679

McKenzie D, O'Nions RK (1991) Partial melt distributions from inversion of rare earth element concentrations. J Petrol 32:1021–1091

McMillan NJ, Dickin AP, Haag D (2000) Evolution of magma source regions in the Rio Grande rift, southern New Mexico. Geol Soc Am Bull 112: 1582–1593

Melluso L, Beccaluva L, Brotzu P, Gregnanin A, Gupta AK, Morbidelli L, Traversa G (1995) Constraints on the mantle sources of the Deccan Traps from the petrology and geochemistry of the basalts of Gujarat state (western India). J Petrol 36:1393–1432

Middlemost EAK (1989) Iron oxidation ratios, norms and the classification of volcanic rocks. Chem Geol 77:19–26

Minster JF, Allègre CJ (1978) Systematic use of trace elements in igneous processes Part III Inverse problem of batch partial melting in volcanic suites. Contrib Mineral Petrol 68:37–52

Morris PA (1995) Slab melting as an explanation of Quaternary volcanism and seismicity in southwest Japan. Geology 23:395–398

Morton-Bermea O (1990) Zur petrologie des alkaligesteins-intrusivkomplexes der Sierra de Picachos (Nuevo León, Mexiko). MS thesis, Institut für Petrographie und geochemie, Universität Karlsruhe, 115 pp

Moyer TC, Esperança S (1989) Geochemical and isotopic variations in a bimodal magma system: the Kaiser Spring volcanic field, Arizona. J Geophys Res 94:7841–8759

Mullen ED (1983) $MnO/TiO_2/P_2O_5$: a minor element discrimination for basaltic rocks of oceanic environments and its implications for petrogenesis. Earth Planet Sci Lett 62:53–62

Myers JD, Marsh BD, Sinha AK (1985) Strontium isotopic and selected trace element variations between two Aleutian volcanic centers (Adak and Atka): implications for the development of arc volcanic plumbing systems. Contrib Mineral Petrol 91:221–234

Myers JD, Marsh BD, Frost CD, Linton JA (2002) Petrologic constraints on the spatial distribution of crustal magma chambers, Atka volcanic center, central Aleutian arc. Contrib Mineral Petrol 143:567–586

Nakagawa M, Ishizuka Y, Kudo T, Yoshimoto M, Hirose W, Ishizaki Y, Gouchi N, Katsui Y, Solovyow AW, Steinberg GS, Abdurakhmanov AI (2002) Tyatya volcano, southwestern Kuril arc: recent eruptive activity inferred from widespread tephra. The Island Arc 11:236–254

Negendank JFW, Emmermann R, Krawczyk R, Mooser F, Tobschall H, Werle D (1985) Geological and geochemical investigations on the eastern Trans Mexican Volcanic Belt. Geofis Int 24:477–575

Nelson BK (1995) Fluid flow in subduction zones: evidence from Nd- and Sr-isotope variations in metabasalts of the Franciscan complex, California. Contrib Mineral Petrol 119:247–262

Nelson SA, Gonzalez-Caver E (1992) Geology and K–Ar dating of the Tuxtla volcanic field, Veracruz, Mexico. Bull Volcanol 55:85–96

Nelson SA, Gonzalez-Caver E, Kyser TK (1995) Constraints on the origin of alkaline and calc-alkaline magmas from the Tuxtla Volcanic Field, Veracruz, Mexico. Contrib Mineral Petrol 122:191–211

Nick K (1988) Mineralogische, Geochemische und Petrographische Untersuchungen in der Sierra de San Carlos (Mexiko). Doctoral thesis, Fakultät für Bio- und Geowissenschaften, Universität (TH) Fridericiana Karlsruhe, 167 pp

Nye CJ, Reid MR (1986) Geochemistry of primary and least fractionated lavas from Okmok volcano, central Aleutians: implications for arc magma genesis. J Geophys Res 91:10271–10287

Ohara Y, Fujioka K, Ishizuka O, Ishii T (2002) Peridotites and volcanics from the Yap arc system: implications for tectonics of the southern Philippine Sea plate. Chem Geol 189:35–53

Ormerod DS, Rogers NW, Hawkesworth CJ (1991) Melting in the lithospheric mantle: inverse modelling of alkali-olivine basalts from the Big Pine volcanic field, California. Contrib Mineral Petrol 108, 305–317

Orozco-Esquivel MT (1995) Zur Petrologie des Vulkangebietes von Palma-Sola, Mexiko. Ein Beispiel fuer den Uebergang von anorogenem zu orogenem Vulkanismus. Doctoral thesis, Institut für Petrographie und Geochemie, Universität Karlsruhe, 167 pp

Pardo M, Suárez G (1995) Shape of the subducted Rivera and Cocos plates in southern Mexico: seismic and tectonic implications. J Geophys Res 100:12357–12373

Patchett PJ, Ruiz J (1987) Nd isotopic ages of crust formation and metamorphism in the Precambrian of eastern and southern Mexico. Contrib Mineral Petrol 96:523–528

Peacock SM (1990) Fluid processes in subduction zones. Science 248: 329–337

Peacock SM, Rushmer T, Thompson AB (1994) Partial melting of subducting oceanic crust. Earth Planet Sci Lett 121:227–244

Pearce JA (1982) Trace element characteristics of lavas from destructive plate boundaries. In: Thorpe RS (ed) Andesites. Wiley, Chichester, pp 525–548

Pearce JA, Cann JR (1973) Tectonic setting of basic volcanic rocks determined using trace element analyses. Earth Planet Sci Lett 19: 290–300

Pearce JA, Gale GH (1977) Identification of ore-deposition environment from trace element geochemistry of associated igneous host rocks. Geol Soc Spec Publ 7:14–24

Pearce JA, Norry MJ (1979) Petrogenetic implications of Ti, Zr, Y, and Nb variations in volcanic rocks. Contrib Mineral Petrol 69:33–47

Pearce JA, Parkinson IJ (1993) Trace element models for mantle melting: application to volcanic arc petrogenesis. In: Prichard HM, Alabaster T, Harris NBW, Neary CR (eds) Magmatic processes and plate tectonics. Geol Soc London Spec Publ 76:373–403

Pearce JA, Peate DW (1995) Tectonic implications of the composition of volcanic arc magmas. Annu Rev Earth Planet Sci 23:251–285

Peate D, Hawkesworth CJ (1996) Lithospheric to asthenospheric transition in low-Ti flood basalts from southern Paraná, Brazil. Chem Geol 127: 1–24

Peng ZC, Zartman RE, Futa K, Chen DG (1986) Pb-, Sr- and Nd-isotopic systematics and chemical characteristics of Cenozoic basalts, eastern China. Chem Geol 59:3–33

Peng ZX, Mahoney J, Hooper P, Harris C, Beane J (1994) A role for lower continental crust in flood basalt genesis? Isotopic and incompatible study of the lower six formations of the western Deccan traps. Geochim Cosmochim Acta 58:267–288

Perry FV, Baldridge WS, DePaolo DJ, Shafiqullah M (1990) Evolution of a magmatic system during continental extension: the mount Taylor volcanic field, New Mexico. J Geophys Res 95:19327–19348

Perterman M, Hirschmann MM, Hametner K, Günther D, Schmidt MW (2004) Experimental determination of trace element partitioning between garnet and silica-rich liquid during anhydrous partial melting of MORB-like eclogite. Geochem Geophys Geosys 4:Q05A01. DOI 10.1029/2003GC000638

Petford N, Gallahar K (2001) Partial melting of mafic (amphibolitic) lower crust by periodic influx of basaltic magma. Earth Planet Sci Lett 193:483–499

Pichler H, Weyl R (1976) Quaternary alkaline volcanic rocks in Eastern Mexico and Central America. Münster Forsch Geol Palaeont 38–39:159–178

Plank T, Langmuir CH (1993) Tracing trace elements from sediment input to volcanic output at subduction zones. Nature 362:739–743

Proteau G, Scaillet B, Pichavant M (1999) Fluid-present melting of ocean crust in subduction zones. Geology 27:1111–1114

Ramírez-Fernández JA (1996) Zur petrogenese des alkalikomplexes der Sierra de Tamaulipas, NE-Mexiko, Geowissenschaftlichen Fakutät, Albert-Ludwigs-Universität, Freiburg, Germany, 316 pp

Raos AM, Crawford AJ (2004) Basalts from the Afate Island group, central section of the Vanuatu arc, SW Pacific: geochemistry and petrogenesis. J Volcanol Geotherm Res 134:35–56

Roberts SJ, Ruiz J (1989) Geochemistry of exposed granulite facies terrains and lower crustal xenoliths in Mexico. J Geophys Res 94: 7961–7974

Robin C (1976) Présence simultanée de magmatismes de significations tectoniques opposées dans l'Est du Mexique. Bull Soc Géol France 18: 1637–1645

Robin C (1982a) Mexico. In: Thorpe RS (ed) Andesites. Wiley, Chichester, pp 137–147

Robin C (1982b) Relations volcanologie-magmatologie-géodynamique: application au passage entre volcanismes alcalin et andésitique dans le sud Mexicain (Axe Trans-mexicain et Province Alcaline Orientale). Annales Scientifiques de l'Universite de Clermont-Ferrand II 31:503

Robin C, Tournon J (1978) Spatial relations of andesitic and alkaline provinces in Mexico and Central America. Can J Earth Sci 15:1633–1641

Rogers G, Saunders AD, Terrell DJ, Verma SP, Marriner GF (1985) Geochemistry of Holocene volcanic rocks associated with ridge subduction in Baja California, Mexico. Nature 315:389–392

Rollinson HR (1993) Using geochemical data: evaluation, presentation, interpretation. Longman Scientific Technical, Essex, 344 pp

Romick JD, Perfit MR, Swanson SE, Shuster RD (1990) Magmatism in the eastern Aleutian arc: temporal characteristic of igneous activity on Akutan Island. Contrib Mineral Petrol 104:700–721

Rudnick RL (1992) Xenoliths–samples of the lower continental crust. In: Fountain DM, Arculus R, Kay RW (eds) Continental lower crust. Elsevier, Amsterdam, pp 269–316

Ruiz J, Patchett PJ, Arculus RJ (1988a) Nd–Sr isotope composition of lower crustal xenoliths—evidence for the origin of mid-Tertiary felsic volcanics in Mexico. Contrib Mineral Petrol 99:36–43

Ruiz J, Patchett PJ, Ortega-Gutierrez F (1988b) Proterozoic and Phanerozoic basement terranes of Mexico from Nd isotopic studies. Geol Soc Am Bull 100:274–281

Sakuyama M, Nesbitt RW (1986) Geochemistry of the Quaternary volcanic rocks of the Northeast Japan arc. J Volcanol Geotherm Res 29:413–450

Sato H (1977) Nickel content of basaltic magmas: identification of primary magmas and a measure of the degree of olivine fractionation. Lithos 10:113–120

Saunders AD, Rogers G, Marriner GF, Terrell DJ, Verma SP (1987) Geochemistry of Cenozoic volcanic rocks, Baja California, Mexico: implications for the petrogenesis of post-subduction magmas. J Volcanol Geotherm Res 32:223–245

Schaaf P, Heinrich W, Besch T (1994) Composition and Sm-Nd isotopic data of the lower crust beneath San Luis Potosí, central Mexico: evidence from a granulite-facies xenolith suite. Chem Geol 118:63–84

Shervais JW (1982) Ti–V plots and the petrogenesis of modern and ophiolitic lavas. Earth Planet Sci Lett 59:101–118

Siebert L, Carrasco-Núñez G (2002) Late-Pleistocene to preColumbian behind-the-arc mafic volcanism in the eastern Mexican Volcanic Belt; implications for future hazards. J Volcanol Geotherm Res 115:179–205

Singer BS, Kudo AM (1986) Assimilation-fractional crystallization of Polvadera Group rocks in the northwestern Jemez volcanic field, New Mexico. Contrib Mineral Petrol 94:374–386

Singer BS, Myers JD, Frost CD (1992) Mid-Pleistocene basalt from the Seguam volcanic center, central Aleutian arc, Alaska: local lithospheric structures and source variability in the Aleutian arc. J Geophys Res 97: 4561–4578

Singh SK, Pardo M (1993) Geometry of the Benioff zone and state of stress in the overriding plate in central Mexico. Geophys Res Lett 20:1483–1486

Sisson TW, Bronto S (1998) Evidence for pressure-release melting beneath magmatic arcs from basalt at Galunggung, Indonesia. Nature 391: 883–886

Smellie JL (1983) A geochemical overview of subduction-related igneous activity in the South Shetland islands, Lesser Antarctica. In: Oliver RL, James PR, Jago JB (eds) Antarctic earth science. Australian Academy of Sciences and Cambridge University Press, Cambridge, pp 352–356

Smith TE, Thirlwall MF, MacPherson C (1996) Trace element and isotope geochemistry of the volcanic rocks of Bequia, Grenadine Islands, Lesser Antilles Arc: a study of subduction enrichment and intra-crustal contamination. J Petrol 37:117–143

Smith EI, Sánchez A, Walker JD, Wang K (1999) Geochemistry of mafic magmas in the Hurricane Volcanic Field, Utah: implications of small- and large-scale chemical variability of the lithospheric mantle. J Geol 107:433–448

Stephenson D, Marshall TR (1984) The petrology and mineralogy of Mt. Popa volcano and the nature of the late-Cenozoic Burma volcanic arc. J Geol Soc London 141:747–762

Stern CR, Frey FA, Futa K, Zartman RE, Peng Z, Kyser TK (1990) Trace-element and Sr, Nd, Pb, and O isotopic composition of Pliocene and Quaternary alkali basalts of the Patagonian Plateau lavas of southernmost South America. Contrib Mineral Petrol 104:294–308

Stolz AJ, Varne R, Wheller GE, Foden JD, Abbott MJ (1988) The geochemistry and petrogenesis of K-rich alkaline volcanics from the Batu Tara volcano, eastern Sunda arc. Contrib Mineral Petrol 98:374–389

Stolz AJ, Varne R, Davies GR, Wheller GE, Fodon JD (1990) Magma source components in an arc-continent collision zone: the Flores-Lembata sector, Sunda arc, Indonesia. Contrib Mineral Petrol 105:585–601

Storey M, Rogers G, Saunders AD, Terrell DJ (1989) San Quintín volcanic field, Baja California, Mexico: 'within plate' magmatism following ridge subduction. Terra Nova 1:195–202

Sun S-S, McDonough WF (1989) Chemical and isotopic systematics of oceanic basalts: implications for mantle composition and processes. In: Saunders AD, Norry MJ (eds) Magmatism in the ocean basins. Geol Soc Spec Publ 42:313–345

Tamura Y (1994) Genesis of island arc magmas by mantle derived bimodal magmatism: evidence from the Shiraham group, Japan. J Petrol 35:619–645

Tatsumi Y, Sakuyama M, Fukuyama H, Kushiro I (1983) Generation of arc basalt magmas and thermal structure of the mantle wedge in subduction zones. J Geophys Res 88:5815–5825

Tatsumi Y, Murasaki M, Arsadi EM, Nohda S (1991) Geochemistry of Quaternary lavas from NE Sulawesi: transfer of subduction components into the mantle wedge. Contrib Mineral Petrol 107:137–149

Tatsumi Y, Murasaki M, Nohda S (1992) Across-arc variation of lava chemistry in the Izu-Bonin arc: identification of subduction components. J Volcanol Geotherm Res 49:179–190

Taylor SR, McLennan SM (1985) The continental crust: its composition and evolution. Blackwell Scientific, Oxford, 312 pp

Taylor RN, Nesbitt RW (1998) Isotopic characteristics of subduction fluids in an intra-oceanic setting, Izu-Bonin Arc, Japan. Earth Planet Sci Lett 164:79–98

Thirlwall MF, Graham AM (1984) Evolution of high-Ca, high-Sr C-series basalts from Grenada, Lesser Antilles: the effects of intra-crustal contamination. J Geol Soc London 141:427–445

Thirlwall MF, Graham AM, Arculus RJ, Harmon RS, Macpherson CG (1997) Resolution of the effects of crustal assimilation, sediment subduction, and fluid transport in island arc magmas: Pb-Sr-Nd-O isotope geochemistry of Grenada, Lesser Antilles. Geochim Cosmochim Acta 60: 4785–4810

Thorpe RS (1977) Tectonic significance of alkaline volcanism in eastern Mexico. Tectonophysics 40:T19-T26

Togashi S, Tanaka T, Yoshida T, Ishikawa K-I, Fujinawa A, Kurasawa H (1992) Trace elements and Nd–Sr isotopes of island arc tholeiites from frontal arc of northeast Japan. Geochem J 26:261–277

Tormey DR, Hickey-Vargas R, Frey FA, López-Escobar L (1991) Recent lavas from the Andean volcanic front (33 to 42°S); interpretations of along-arc compositional variations. In: Harmon RS, Rapela CW (eds) Andean magmatism and its tectonic setting. Geol Soc Am Spec Pap 265: 57–77

Torres-Alvarado IS, Verma SP, Palacios-Berruete H, Guevara M, González-Castillo OY (2003) DC_Base: a database system to manage Nernst distribution coefficients and its application to partial melting modeling. Comput Geosci 29:1191–1198

Treviño-Cázares A, Ramírez-Fernández JA, Velasco-Tapia F, Rodríguez-Saavedra P (2005) Mantle xenoliths and their host magmas in the Eastern Alkaline Province (NE Mexico). Int Geol Rev 47:1260–1286

Trua T, Deniel C, Mazzuoli R (1999) Crustal control in the genesis of Plio-Quaternary bimodal magmatism of the Main Ethiopian Rift (MER): geochemical and isotopic (Sr, Nd, Pb) evidence. Chem Geol 155:201–231

Turner S, Foden J (2001) U, Th and Ra disequilibria, Sr, Nd and Pb isotope and trace element variations in Sunda arc lavas: predominance of a subducted sediment component. Contrib Mineral Petrol 142:43–57

Turner S, McDermott F, Hawkesworth C, Kepezhinskas P (1998) A U-series study of lavas from Kamchatka and the Aleutians: constraints on source composition and melting processes. Contrib Mineral Petrol 133:217–234

Turner S, Foden J, George R, Evans P, Varne R, Elburg M, Jenner G (2003) Rates and processes of potassic magma evolution beneath Sangeang Api volcano, East Sunda arc, Indonesia. J Petrol 44:491–515

Vasconcelos-F. M, Verma SP, Rodríguez-G. JF (1998) Discriminación tectónica: nuevo diagrama Nb–Ba para arcos continentales, arcos insulares, "rifts" e islas oceánicas en rocas máficas. Bol Soc Esp Min 21:129–146

Velasco-Tapia F, Verma SP (2001) First partial melting inversion model for a rift-related origin of the Sierra de Chichinautzin volcanic field, central Mexican Volcanic Belt. Int Geol Rev 43:788–817

Verma SP (1983) Magma genesis and chamber processes at Los Humeros caldera, Mexico—Nd and Sr isotope data. Nature 301:52–55

Verma SP (1984) Alkali and alkaline earth element geochemistry of Los Humeros caldera, Puebla, Mexico. J Volcanol Geotherm Res 20:21–40

Verma SP (1991) Usefulness of liquid chromatography for determination of thirteen rare-earth elements in rocks and minerals. Lanthan Actin Res 3: 237–257

Verma SP (1992) Seawater alteration effects on REE, K, Rb, Cs, Sr, U, Th, Pb and Sr–Nd–Pb isotope systematics in Mid-Ocean Ridge Basalt. Geochem J 26:159–177

Verma SP (2000a) Geochemical evidence for a lithospheric source for magmas from Los Humeros caldera, Puebla, Mexico. Chem Geol 164:35–60

Verma SP (2000b) Geochemistry of the subducting Cocos plate and the origin of subduction-unrelated mafic volcanism at the volcanic front of the central Mexican Volcanic Belt. In: Delgado-Granados H, Aguirre-Díaz G, Stock JM (eds) Cenozoic tectonics and volcanism of Mexico. Geol Soc Am Spec pap 334:195–222

Verma SP (2001) Geochemical evidence for a lithospheric source for magmas from Acoculco caldera, eastern Mexican Volcanic Belt. Int Geol Rev 43:31–51

Verma SP (2002) Absence of Cocos plate subduction-related basic volcanism in southern Mexico: a unique case on Earth? Geology 30: 1095–1098

Verma SP (2004) Solely extension-related origin of the eastern to west-central Mexican Volcanic Belt (Mexico) from partial melting inversion model. Curr Sci 86:713–719

Verma SP, Lopez MM (1982) Geochemistry of Los Humeros caldera, Puebla, Mexico. Bull Volcanol 45:63–79

Verma SP, Nelson SA (1989) Isotopic and trace element constraints on the origin and evolution of alkaline and calc-alkaline magmas in the northwestern Mexican Volcanic Belt. J Geophys Res 94:4531–4544

Verma SP, Besch T, Guevara M, Schulz-Dobrich B (1992) Determination of twelve trace elements in twenty-seven and ten major elements in twenty-three geochemical reference samples by X-ray fluorescence spectrometry. Geostand Newslett 16:301–309

Verma SP, Salazar VA, Negendank JFW, Milán M, Navarro LI, Besch T (1993) Características petrográficas y geoquímicas de elementos mayores del campo volcánico de Los Tuxtlas, Veracruz, México. Geofís Int 32:237–248

Verma SP, Orduña-Galván LJ, Guevara M (1998) SIPVADE: a new computer programme with seventeen statistical tests for outlier detection in evaluation of international geochemical reference materials and its application to Whin Sill dolerite WS-E from England and Soil-5 from Peru. Geostand Newslett J Geostand Geoanal 22:209–234

Verma SP, Torres-Alvarado IS, Sotelo-Rodríguez ZT (2002) SINCLAS: standard igneous norm and volcanic rock classification system. Comput Geosci 28:711–715

Walker JA, Patino LC, Carr MJ, Feigenson MD (2001) Slab control over HFSE depletions in central Nicaragua. Earth Planet Sci Lett 192:533–543

Wang K, Plank T, Walker JD, Smith EI (2002) A mantle melting profile across the Basin and Range, SW USA. J Geophys Res 107:ECV 5-1–5-21

Weaver BL (1991) The origin of ocean island basalt end-member compositions: trace element and isotopic constraints. Earth Planet Sci Lett 104:381–397

Weaver BL, Tarney J (1984) Empirical approach to estimating the composition of the continental crust. Nature 310:575–577

Werner R, Hoernle K, Barckhausen U, Hauff F (2003) Geodynamic evolution of the Galápagos hot spot system (Central East Pacific) over the past 20 m.y.: constraints from morphology, geochemistry, and magnetic anomalies. Geochem Geophys Geosyst 4:1108. DOI 10.1029/2003GC000576

van Westrenen W, Blundy JD, Wood BJ (2001) High field strength element/rare earth element fractionation during partial melting in the presence of garnet: implications for identification of mantle heterogeneities. Geochem Geophys Geosyst 2:2000GC000133

Wheller GE, Varne R, Foden JD, Abbott MJ (1987) Geochemistry of Quaternary volcanism in the Sunda-Banda arc, Indonesia, and three-component genesis of island-arc basaltic magmas. J Volcanol Geotherm Res 32:137–160

White WM, Dupré B (1986) Sediment subduction and magma genesis in the Lesser Antilles: isotopic and trace element constraints. J Geophys Res 91:5927–5941

White WM, Patchett J (1984) Hf–Nd–Sr isotopes and incompatible element abundances in island arcs: implications for magma origins and crust-mantle evolution. Earth Planet Sci Lett 67:167–185

Whitford DJ, Nicholls IA, Taylor SR (1979) Spatial variations in the geochemistry of Quaternary lavas across the Sunda arc in Java and Bali. Contrib Mineral Petrol 70:341–356

Wilcox RE (1999) The idea of magma mixing: history of a struggle for acceptance. J Geol 107:421–432

Williamson M-C, Courtney RC, Keen CE, Dehler SA (1995) The volume and rare earth concentrations of magmas generated during finite stretching of the lithosphere. J Petrol 36:1433–1453

Wilson M (1989) Igneous petrogenesis. A global tectonic approach. Harper Collins Academic, London, 456 pp

Wilson M, Downes H (1991) Tertiary–Quaternary extension-related alkaline magmatism in western and central Europe. J Petrol 32:811–849

Wood DA (1980) The application of a Th–Hf–Ta diagram to problems of tectonomagmatic classification and to establishing the nature of crustal contamination of basaltic lavas of the British Tertiary volcanic province. Earth Planet Sci Lett 50:11–30

Woodhead JD (1988) The origin of geochemical variations in Mariana lavas: a general model for petrogenesis in intra-oceanic island arcs. J Petrol 29:805–830

Woodhead JD, Johnson RW (1993) Isotopic and trace-element profiles across the New Britain island arc, Papua New Guinea. Contrib Mineral Petrol 113:479–491

Yogodzinski GM, Kay RW, Volynets ON, Koloskov AV, Kay SM (1995) Magnesian andesite in the western Aleutian Komandorsky region: implications for slab melting and processes in the mantle wedge. Geol Soc Am Bull 107:505–519

Zhang M, Suddaby P, Thompson RN, Thirlwall MF, Menzies MA (1995) Potassic volcanic rocks in NE China: geochemical constraints on mantle source and magma genesis. J Petrol 36:1275–1303

Zhi X, Song Y, Frey FA, Feng J, Zhai M (1990) Geochemistry of Hannuoba basalts, eastern China: constraints on the origin of continental alkalic and tholeiitic basalt. Chem Geol 88:1–33

Zhuravlev DZ, Tsvetkov AA, Zhuravlev AZ, Gladkov NG, Chernysheva IV (1987) $^{143}Nd^{144}Nd$ and $^{87}Sr^{86}Sr$ ratios in recent magmatic rocks of the Kurile Island Arc. Chem Geol 66:227–243

Zindler A, Hart S (1986) Chemical geodynamics. Annu Rev Earth Planet Sci 14:493–571

Zindler A, Staudigel H, Batiza R (1984) Isotope and trace element geochemistry of young Pacific seamounts: implications for the scale of upper mantle heterogeneity. Earth Planet Sci Lett 70:175–195

Zou H, Zindler A, Xisheng X, Qi Q (2000) Major, trace element, and Nd, Sr and Pb isotope studies of Cenozoic basalts in SE China: mantle sources, regional variations and tectonic significance. Chem Geol 171:33–47